



## REVIEW

[View Article Online](#)  
[View Journal](#) | [View Issue](#)

 Cite this: *Mater. Chem. Front.*,  
 2023, 7, 4723

# Electronic and geometric modulations of catalysts for electrochemical CO<sub>2</sub> reduction reaction

 Shilin Wei, Weiqi Liu,\* Chuangchuang Yang, Peiyao Bai, Xiao Kong, Wenbo Sun   
 and Lang Xu \*

The electrocatalytic CO<sub>2</sub> reduction reaction (CO<sub>2</sub>RR) converts CO<sub>2</sub> into high-value-added chemicals using clean and renewable energy, making it one of the most promising strategies for addressing present-day energy and environmental crises. Electrocatalysts play a crucial role in electrocatalytic CO<sub>2</sub>RR systems because they determine catalytic activities and selectivities. Electronic and geometric structures are two important factors that affect the electrocatalytic performances of electrocatalysts, in which the electronic structures are related to the adsorption strengths of substrates/intermediates while the geometric structures are associated with the microenvironments of catalytic reactions. Consequently, modulating the electronic and/or geometric structures of electrocatalysts can significantly improve the catalytic performances. To better understand the roles and importance of electronic and geometric structural modulations, this review systematically summarizes and discusses the latest progress of these two strategies that apply to electrocatalytic CO<sub>2</sub>RRs. First, the methods for electronic and geometric structural modulations of electrocatalysts are introduced. Then, the trends and mechanisms of electronic structural modulation of various metal elements are explored in detail based on element partitioning across the periodic table, starting with the s- and p-block elements and ending with broad coverage of the d- and f-block metals, and the advantages and functions of geometric structural modulation of catalyst supports and the impact mechanism on performance are discussed according to types of supports. Finally, some prospects are proposed to provide suggestions for designing more efficient electrocatalysts for the electrocatalytic CO<sub>2</sub>RR based on these two strategies.

 Received 7th April 2023,  
 Accepted 28th June 2023

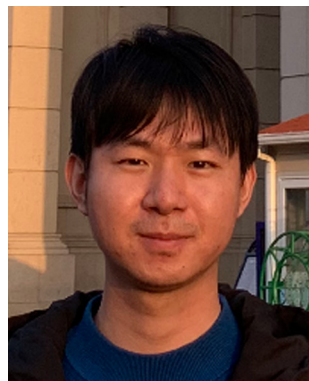
DOI: 10.1039/d3qm00364g

[rsc.li/frontiers-materials](https://rsc.li/frontiers-materials)

## 1. Introduction

The fast development in modern industry accelerates the progress of society, but at the same time, it also consumes a lot of fossil fuels (such as natural gas, petroleum, and coal), resulting in an enormous amount of CO<sub>2</sub> being emitted into the

MOE Key Laboratory of Coal Processing and Efficient Utilization, School of Chemical Engineering and Technology, China University of Mining and Technology, 1 Daxue Road, Xuzhou, Jiangsu 221116, China. E-mail: lang.xu@cumt.edu.cn, weiqi.liu@cumt.edu.cn



Shilin Wei

Shilin Wei received his BEng degree from China University of Mining and Technology in 2020 and is now a doctoral student at the same university. His research interests focus on the reaction mechanisms of carbon dioxide reduction reaction via multi-physical field coupling and the modelling of electrochemical energy conversions.



Weiqi Liu

Weiqi Liu received his bachelor's and master's degrees from Shandong University of Technology and his doctoral degree from China University of Mining and Technology in 2023. He is now a postdoctoral researcher associate at China University of Mining and Technology. His major research interests include preparations of coal-based functional materials and electrocatalytic reduction of carbon dioxide.

atmosphere.<sup>1–4</sup> At present, the concentration of CO<sub>2</sub> in the atmosphere has reached 420 ppm, which is higher than the safe level of 350 ppm.<sup>5,6</sup> The excessive CO<sub>2</sub> has triggered the global greenhouse effect, leading to glacial ablation, rising sea levels, climate anomalies, species extinction, and other serious issues.<sup>7–11</sup> Therefore, it is crucial to overcome the CO<sub>2</sub> issues.<sup>12–15</sup>

Among numerous schemes, the electrochemical CO<sub>2</sub> reduction reaction (CO<sub>2</sub>RR) is particularly attractive, since it can not only directly use the electricity generated by renewable energy to drive the entire electrocatalytic system but also flexibly regulate the types and yields of reduction products by adjusting external parameters.<sup>16–22</sup> In addition, the electrochemical systems can be operated in aqueous solutions (providing protons) at normal temperature and pressure, which is beneficial to improving energy efficiencies and therefore providing sustainable development paths for a low-carbon society.<sup>23–26</sup> In recent decades, researchers have made great efforts to expand and optimize CO<sub>2</sub>RR technologies. A substantial number of high-performance catalysts have been developed, such as single-atom catalysts,<sup>27,28</sup> hierarchical nanosheet catalysts,<sup>29</sup> 3D nanosheet arrays,<sup>30</sup> nano-polyaniline catalysts,<sup>31</sup> porous hollow Cu microspheres catalysts,<sup>32</sup> and metallic oxide catalysts.<sup>33</sup> Not only have various structures and types of electrocatalysts been prepared, but also the conversion mechanisms of

CO<sub>2</sub> molecules on a vast array of catalytically active sites have been intensively studied using state-of-the-art characterization and theoretical calculation methods.<sup>34–39</sup> Since heterogeneous catalysts can be directly coated on electrically conducting catalyst supports, the efficient charge transfer between catalysts and supports enables the former to exhibit relatively high activities. At the same time, heterogeneous catalysts are ready for reuse, which greatly improves economic efficiencies.<sup>40–43</sup> As heterogeneous catalysts are advantageous in the electrocatalytic CO<sub>2</sub>RR, we limit the research scope to this class of electrocatalysts in this review.

Traditional electrocatalysts show relatively low product selectivities and current densities for the CO<sub>2</sub>RR, which are mainly attributed to their weak adsorptions (including adsorption strengths and capacities) to CO<sub>2</sub>/intermediates.<sup>44,45</sup> The electronic structures of active sites of these electrocatalysts are quite stable, making it difficult to couple the outer orbitals of the active sites with the substrate or intermediate molecules and thus resulting in the weak adsorption strengths between electrocatalysts and CO<sub>2</sub>/intermediates.<sup>6,46</sup> On the other hand, the catalyst supports that possess smooth surfaces and lack porous structures would have low adsorption capacities for CO<sub>2</sub>/intermediates, which impedes the prompt supply of reaction substrate molecules to active sites and therefore greatly limits the resulting electrocatalytic activities.<sup>45–47</sup>



**Chuangchuang Yang**

*Chuangchuang Yang received his BSc degree from China University of Mining and Technology in 2019. At present, he is pursuing his doctoral degree at the same institute. His current research interests concentrate on the construction and exploration of electrocatalysts toward CO<sub>2</sub> and O<sub>2</sub> reduction reactions.*



**Peiyao Bai**

*Peiyao Bai received his BSc degree from China University of Mining and Technology in 2018. After that, he continued to pursue his doctoral degree at the same university. Now his research interests are mainly in the green synthesis of value-added chemicals via electrochemical routes, advanced energy-conversion system designs, and a deep understanding of electrochemical processes in multi-phase interfaces.*



**Xiao Kong**

*Xiao Kong received his bachelor's and master's degrees from Shandong University of Technology and is now a doctoral student at China University of Mining and Technology. His research interests involve carbon and nitrogen fixations using electrochemical methods.*

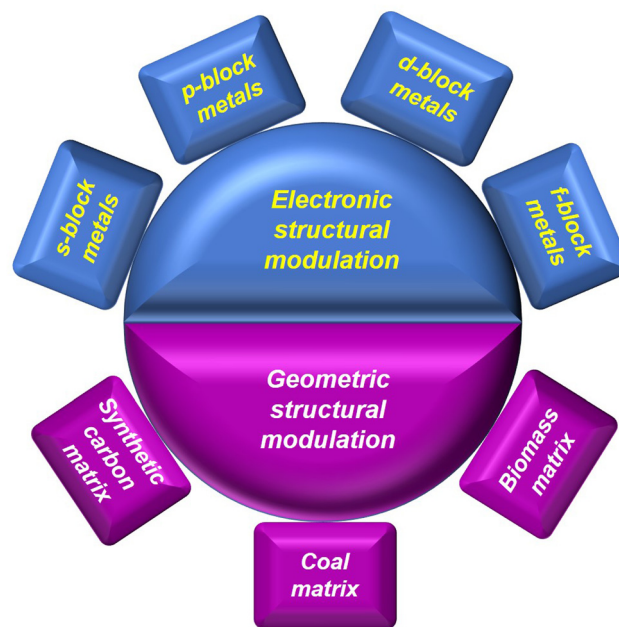


**Wenbo Sun**

*Wenbo Sun graduated from Henan University of Technology and is currently a master student at China University of Mining and Technology. His main research interests include the synthesis and characterization of biomass-based metal-free electrocatalysts for the carbon dioxide reduction reaction.*

Consequently, the electronic structures of metal sites and the geometric structures of supports are the two key factors in determining the CO<sub>2</sub>RR performance of electrocatalysts, and the electrocatalytic activities can be therefore strengthened from these two aspects: electronic structural modulation of active sites and geometric structural modulation of supports. Electronic structural modulation commonly utilizes foreign active species to disturb the electronic configurations of host metal species.<sup>48–51</sup> The resulting overlap and distortion of electron densities can change the binding strengths between electrocatalysts and CO<sub>2</sub>/intermediates.<sup>6</sup> Accordingly, the precise electronic structural modulation enables electrocatalysts to obtain optimized adsorption strengths for CO<sub>2</sub>/intermediates, thereby capable of improving the catalytic activities and selectivities. Moreover, the geometric structural modulation usually optimizes the porous structures and morphologies of catalyst supports, which allows them not only to adsorb a large amount of CO<sub>2</sub>/intermediates but also to expose as many active sites as possible.<sup>52–55</sup> In addition, the size effects of the geometric structures of supports can further optimize the catalytic rates.<sup>24,56,57</sup> This is why electronic and geometric structural modulations are the two effective strategies to synthesize efficient CO<sub>2</sub>RR electrocatalysts.

Many reviews regarding the CO<sub>2</sub>RR have been published according to different emphases and topics to date, such as fundamentals and industrialization of the CO<sub>2</sub>RR,<sup>58</sup> CO<sub>2</sub>RR pathways,<sup>59</sup> single-atom catalysts,<sup>60</sup> copper-based catalysts,<sup>61</sup> *in situ* dynamic studies,<sup>62</sup> CO<sub>2</sub>RR selectivity,<sup>63</sup> and catalyst interface engineering.<sup>64</sup> However, an overview of electronic and geometric structural modulations in terms of CO<sub>2</sub>RR is lacking. In this sense, it is timely to make a comprehensive and systematic summary regarding the electronic and geometric structural modulations toward the CO<sub>2</sub>RR. Because the electronic and geometric structural modulation can regulate the electrocatalytic performances from microscopic perspectives, it is convenient for researchers to explore the structure–activity relationships and reveal the underlying reaction mechanisms. Moreover, the electronic and geometric structural modulations



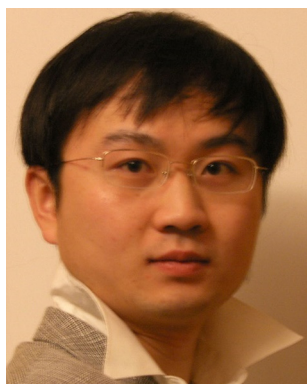
Scheme 1 Strategies of electronic and geometric structural modulations.

are applicable to various types and scales of CO<sub>2</sub>RR electrocatalysts, and this broad application capability can facilitate the development of catalyst diversity. Therefore, in view of the importance of electronic and geometric structural modulations for the enhancement of catalyst performance as well as the lack of systematic reviews about these two strategies, we now summarize the recent progress of CO<sub>2</sub>RR electrocatalysts whose electronic and geometric structures have been modulated.

In this review, the recently reported electronic and geometric structural modulations toward the improvement in electrocatalytic CO<sub>2</sub>RR performances are comprehensively summarized. Scheme 1 illustrates a variety of paths that can be used to optimize CO<sub>2</sub>RR behaviors *via* the two strategies. Moreover, we combine physicochemical characterization with theoretical calculations to probe the mechanisms of action for the effects of electronic and geometric structural modulations on electrocatalyst performance. Finally, an outlook for the future development of CO<sub>2</sub>RR electrocatalysts is presented in light of these two modulation strategies. We hope that this review proves to be stimulating and provides inspiration for researchers to develop high-performance electrocatalysts toward the CO<sub>2</sub>RR and other related reactions.

## 2. Electronic structural modulation

According to the Sabatier principle, electrocatalysts with excellent CO<sub>2</sub>RR performance should have optimum adsorption strengths between their active sites and CO<sub>2</sub>/intermediates.<sup>44</sup> It is found that the electronic structures of active sites strongly determine the adsorption states of CO<sub>2</sub>/intermediates. Therefore, modulating the electronic structures of active sites can optimize the adsorption strengths of the reaction substrates and intermediates.<sup>6,44,46</sup> Because of the difference



Lang Xu

*Lang Xu graduated with a BSc degree from Nanjing University and a DPhil degree from University of Oxford under the supervision of Professor Fraser A. Armstrong FRS, and is now a Professor of Chemistry at China University of Mining and Technology. He is mainly engaged in research in the fields of green and low-carbon energy molecular science and engineering, including carbon dioxide resource utilization, fuel cells, coal/biomass-based electrocatalytic materials, and molecular modelling.*

in electronegativity among various elements, atoms with higher electronegativity tend to attract electrons of those with lower electronegativity, resulting in the delocalization of valence electrons. Thus, introducing a second metal species into the host metal can effectively modulate the electronic structure of the latter.<sup>65–67</sup> More importantly, the electronegativity difference between the second metal species and the host can regulate the density of states in the vicinity of the Fermi level, which is conducive to enhancing the activity of electrons in the outer orbitals of active sites.<sup>68–70</sup> Therefore, utilizing the second species to precisely modulate the electronic structure of the host enables electrocatalysts to obtain the optimum adsorption strengths for CO<sub>2</sub>/intermediates, thereby achieving high activities and selectivities.<sup>48,50</sup> Furthermore, the electronic structural modulation can break the linear scale relationship (*i.e.*, the adsorption energy of one intermediate has a linear scaling relationship with that of its subsequent intermediate on the same active site), contributing to the diversity of products.<sup>44,46</sup> Table 1 summarizes the performances of typical CO<sub>2</sub>RR electrocatalysts whose electronic structures were modulated. We now give detailed descriptions of the electronic structural modulations, which are arranged in the order of s-, p-, d-, and f-blocks.

## 2.1 s-Block metals

s-Block metals, including alkali metals and alkaline earth metals, are a class of metals in which the last electron is filled into the s orbitals. In addition, they are abundant in the Earth's crust, but all exist in the oxidized states (specifically, cations). Because the dissociation energies of electrons in the outermost s orbitals of their metallic states are quite small, the s-block metals tend to lose these electrons.<sup>71</sup> Fortunately, this electron-donating ability gives them the property of modulating electronic structures of other metal species. For example, Yan *et al.* developed an electrochemical surface lithiation strategy to modulate the electronic structure of a Sn electrode (Fig. 1a).<sup>72</sup> By combining spectral characterization with theoretical calculations, they found that the Li intercalation induced the strains of surface Sn lattices and the localization of negative charges of Sn atoms. As shown in Fig. 1b, the photon energy of the Sn–Li catalyst was decreased, indicating the electron transfer from Li to Sn. The increased local electron density of the Sn–Li catalyst resulted in the stronger adsorption strength for HCOO\* (the key intermediate of formate/formic acid) compared to the pure Sn catalyst (Fig. 1c), signifying the enhanced intrinsically catalytic activity of Li-modified Sn atoms. Thus, the Sn–Li catalyst

Table 1 Summary of typical CO<sub>2</sub>RR electrocatalysts whose electronic structures were modulated

|                               | Product                                    | Electrocatalyst                                  | Reactor                 | Electrolyte                       | FE <sup>a</sup> (%)     | <i>j</i> <sup>b</sup> (mA cm <sup>-2</sup> ) | <i>E</i> <sup>c</sup> (V vs. RHE) | Ref.  |    |
|-------------------------------|--|--|-------------------------|-----------------------------------|-------------------------|--|-----------------------------------|-------|----|
| s-Block                       | Formate                                    | s-SnLi   | Flow cell               | 1.0 M KOH                         | 92                      | 1000   | -1.2                              | 72    |    |
|                               | C <sub>2+</sub>                            | Mg–Cu  | Flow cell               | 1.0 M KOH                         | 80                      | 650  | -0.69                             | 73    |    |
| p-Block                       | Formate                                    | Basal-oriented Bi NSs                            | Flow cell               | 1.0 M KOH                         | 98                      | 90   | -0.68                             | 75    |    |
|                               | Formate                                    | In-SAs/NC  | H-type cell             | 0.5 M KHCO <sub>3</sub>           | 96                      | 8.87   | -0.65                             | 77    |    |
|                               | Formate                                    | Bi–SnO/Cu form                                   | H-type cell             | 0.1 M KHCO <sub>3</sub>           | 93                      | 12   | -1.7                              | 80    |    |
|                               | Formate                                    | 2.5% Sn-doped Bi <sub>2</sub> O <sub>3</sub> NSs | H-type cell             | 0.5 M KHCO <sub>3</sub>           | 93.4                    | 24.3   | -0.97                             | 81    |    |
|                               | Formate                                    | BOC NSs  | H-type cell             | 0.5 M KHCO <sub>3</sub>           | 98.3                    | 8  | -0.9                              | 82    |    |
|                               | Formate                                    | Bi–Sn/CF   | H-type cell             | 0.5 M KHCO <sub>3</sub>           | 96                      | 58   | -1.1                              | 83    |    |
|                               | Formate                                    | Sn–Bi interface                                  | H-type cell             | 0.5 M KHCO <sub>3</sub>           | 96.4                    | 40   | -0.84                             | 84    |    |
|                               | Formate                                    | Bi <sub>x</sub> Sn <sub>1-x</sub>                | H-type cell             | 0.1 M KHCO <sub>3</sub>           | 78                      | 8  | -1.1                              | 85    |    |
|                               | Formate                                    | Bi–Sn  | H-type cell             | 0.1 M KHCO <sub>3</sub>           | 93.9                    | 9.3  | -1.0                              | 86    |    |
|                               | Formate                                    | SnIn-3   | Flow cell               | 1.0 M KOH                         | 94                      | 236  | -0.98                             | 87    |    |
|                               | Formate                                    | BiIn <sub>5</sub> -Y@C                           | H-type cell             | 0.5 M KHCO <sub>3</sub>           | 97.5                    | 13.5   | -0.86                             | 88    |    |
|                               | d-Block                                    | CO   | Ni–N–C                  | Flow cell                         | 1.0 M KOH               | 91   | 726                               | -1.18 | 8  |
|                               |  | CO   | Fe–N/P–C                | H-type cell                       | 0.5 M KHCO <sub>3</sub> | 98   | 2                                 | -0.45 | 10 |
|                               |  | CO   | NiPACN-low              | H-type cell                       | 0.1 M KHCO <sub>3</sub> | 99   | 8                                 | -0.8  | 21 |
| CO                            |  | Fe <sub>3</sub> C/Fe <sub>1</sub> N <sub>4</sub> | Flow cell               | 1.0 M KHCO <sub>3</sub>           | 88                      | 10   | -0.75                             | 39    |    |
| Formate                       |  | Pb <sub>1</sub> Cu                               | Flow cell               | 0.5 M KHCO <sub>3</sub>           | 92                      | 1000   | -1.0                              | 48    |    |
| CO                            |  | Au <sub>3</sub> Cu                               | H-type cell             | 0.1 M KHCO <sub>3</sub>           | 98                      | 12.5   | -0.7                              | 49    |    |
| CO                            |  | CoCp2@MOF-545-Co                                 | H-type cell             | 0.5 M KHCO <sub>3</sub>           | 97                      | 15   | -0.7                              | 54    |    |
| CO                            |  | Zn–Cu (5 s)                                      | Flow cell               | 1.0 M KOH                         | 84                      | 50   | -0.54                             | 65    |    |
| Formate                       |  | ZnIn <sub>2</sub> S <sub>4</sub>                 | Flow cell               | 1.0 M KHCO <sub>3</sub>           | 99.3                    | 300  | -1.2                              | 66    |    |
| CO                            |  | Cu <sub>2</sub> O/CuO@Ni                         | H-type cell             | 0.5 M KHCO <sub>3</sub>           | 95                      | 30   | -1.2                              | 68    |    |
| Formate                       |  | Ag–In–S  | Flow cell               | 1.0 M KOH                         | 94                      | 560  | -0.95                             | 70    |    |
| CO                            |  | A–Ni–NSG   | H-type cell             | 0.5 M KHCO <sub>3</sub>           | 97                      | 36.5   | -0.5                              | 92    |    |
| CO                            |  | Ni–N–MEGO  | H-type cell             | 0.5 M KHCO <sub>3</sub>           | 92.1                    | 53.6   | -0.7                              | 94    |    |
| CO                            |  | Fe <sup>3+</sup> –N–C                            | Flow cell               | 0.5 M KHCO <sub>3</sub>           | 95                      | 94   | -0.45                             | 96    |    |
| CH <sub>4</sub>               |  | Cu <sub>2</sub> O@CuHHTP                         | H-type cell             | 0.1 M KCl/0.1 M KHCO <sub>3</sub> | 73                      | 10.8   | -1.4                              | 98    |    |
| C <sub>2</sub> H <sub>4</sub> |  | KB@Cu <sub>3</sub> (HITP) <sub>2</sub>           | Flow cell               | 1.0 M KOH                         | 51                      | 305  | -0.93                             | 99    |    |
| CO                            |  | 5 nm Ag/C  | H-type cell             | 0.5 M KHCO <sub>3</sub>           | 84.4                    | 4  | -0.75                             | 105   |    |
| CO                            |  | 3D AgAu  | Flow cell               | 1.0 M KHCO <sub>3</sub>           | 90                      | 280  | -1.05                             | 107   |    |
| CH <sub>4</sub>               | <i>t</i> -Cu <sub>2</sub> O                | H-type cell                                      | 0.1 M KHCO <sub>3</sub> | 71                                | 12                      | -1.6   | 110                               |       |    |
| C <sub>2+</sub>               | Ag <sub>65</sub> –Cu <sub>35</sub> LNS-100 | H-type cell                                      | 0.1 M KHCO <sub>3</sub> | 72                                | 3.6                     | -1.2   | 112                               |       |    |
| C <sub>2+</sub>               | CuNi-2                                     | Flow cell  | 1.0 M KOH               | 62                                | 227                     | -0.88  | 113                               |       |    |
| C <sub>2-4</sub>              | a-CuTi@Cu                                  | H-type cell                                      | 0.1 M KHCO <sub>3</sub> | 49                                | 1.2                     | -0.8   | 114                               |       |    |
| f-Block                       | CO   | CBNNiGd-700                                      | Flow cell               | 1.0 M KOH                         | 97                      | 308  | -0.91                             | 116   |    |

<sup>a</sup> Faradaic efficiency (FE). <sup>b</sup> Partial current density of products. <sup>c</sup> Applied potential at the highest FE, *versus* reversible hydrogen electrode (RHE, noting that all potentials in this review have been converted to the RHE unless otherwise specified).

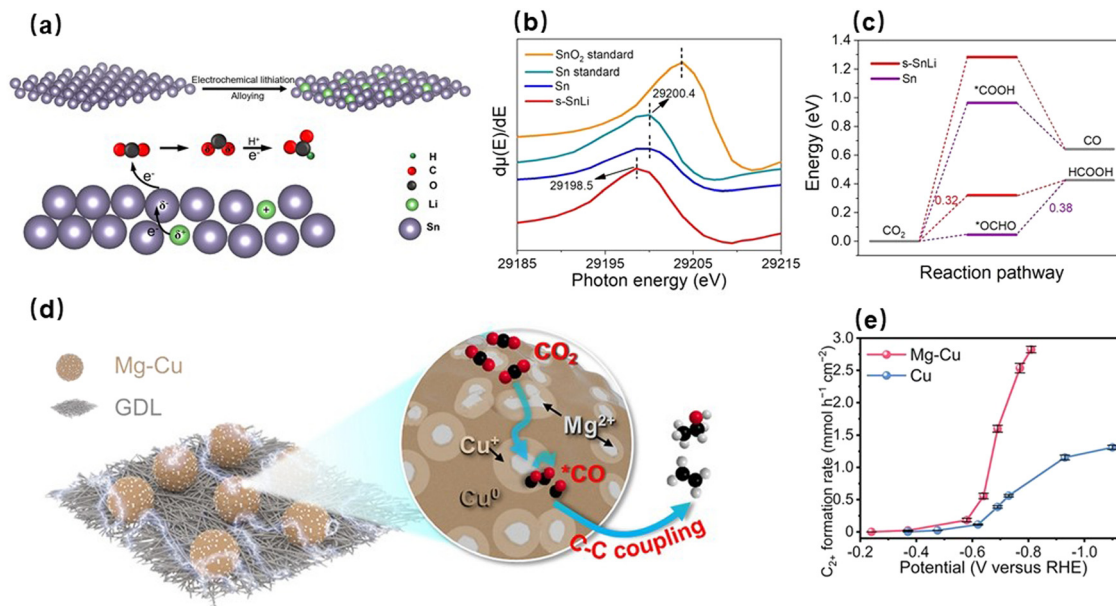


**Fig. 1** (a) Electrochemical lithiation preparation, localization of negative charges, and lattice strains of s-SnLi. (b) Dependence of  $d\mu(E)/dE$  on photon energy for s-SnLi and Sn nanoparticles, alongside SnO<sub>2</sub> and Sn powders. (c) Gibbs free energy of conversions of CO<sub>2</sub> to CO and HCOOH on s-SnLi and Sn.<sup>72</sup> Reproduced with permission from Wiley-VCH Verlag GmbH & Co. KGaA, copyright 2021. (d) A reaction mechanism of CO<sub>2</sub> to C<sub>2+</sub> products on the surface of Mg–Cu. (e) Formation rates of C<sub>2+</sub> products at different potentials for Mg–Cu and Cu.<sup>73</sup> Reproduced with permission from Wiley-VCH Verlag GmbH & Co. KGaA, copyright 2022.

displayed a high formate selectivity of 92% and a high partial current density of 1.0 A cm<sup>-2</sup> at a potential of -1.2 V in a flow cell. Xie *et al.* successfully modified a Cu-based catalyst with Mg. The magnesium ions enhanced the electropositivity of Cu through the interaction with O atoms, significantly increasing the electrocatalytic CO<sub>2</sub>RR activity (Fig. 1d).<sup>73</sup> Compared with the unmodified catalyst, the Mg-modulated catalyst presented an excellent C<sub>2+</sub> faradaic efficiency, and its C<sub>2+</sub> product generation rate was increased by more than 5 times at -0.7 V (Fig. 1e). In addition, Xu *et al.* found that Cu catalysts decorated with alkaline earth metal oxide could improve the FE of CO<sub>2</sub>-to-ethanol by selective hydrogenation.<sup>74</sup> In particular, the FE can reach 61% after BaO modification.

At present, there are very few reports on the use of s-block metals to modulate the electronic structures of host metal atoms. The electrons in the outermost s orbitals of their metallic states are extremely active, making it difficult for the s-block metals to be incorporated into other metal species in a stable state. Nevertheless, the strong electron-donating property of s-block metals makes them possess great development space in the field of electronic structural modulation of metal species.

## 2.2 p-Block metals

p-Block metals with the last electron located in the p orbitals are now widely used for the electrocatalytic CO<sub>2</sub>RR, such as Sn, In, Bi, and Pb, because both p-block metals and their oxides exhibit relatively high selectivities for formate/formic acid.<sup>75–78</sup> Mechanistic studies have shown that the s and p orbitals of the outer layers of p-block metals can be hybridized with the 2p and

2s orbitals of oxygen, which makes p-block metals present the characteristic oxophilicity. Therefore, the p-block metals tend to adsorb CO<sub>2</sub> molecules in the form of oxygen coordination, thus favoring the generation of oxygen-bond intermediates as exemplified by \*OOCH.<sup>79,80</sup> The electronic modulation of p-block metal species can further enhance their selectivities for formate/formic acid. The favorable orbital interactions between two metals (host and guest) can promote the upshift of density of states for host metal active sites, which is beneficial to reducing the bonding states and increasing the antibonding states and thereby enhancing the adsorption of active sites to CO<sub>2</sub>/intermediates.<sup>81,82</sup> For example, Wen *et al.* used Bi nanoparticles to modify Sn nanosheets for highly selective CO<sub>2</sub>RR toward formate (Fig. 2a).<sup>83</sup> The incorporation of Bi not only reduced the local electron density of Sn but also pulled the p and d orbitals of Sn atoms upward from the Fermi level (Fig. 2b and c). Hence, this interaction allowed the electron density of O atoms with the high electronegativity to easily enter the p and d orbitals of Sn atoms, which in turn boosted the bonding of Sn atoms with CO<sub>2</sub> and HCOO\* and improved the selectivity of formate production. Ren *et al.* employed *in situ* electrodeposition to construct Sn–Bi bimetallic interface-rich materials (Fig. 2d).<sup>84</sup> The abundant interfaces between Sn and Bi were highly favorable for the flow of electron density from Sn to Bi. Furthermore, the strong electrostatic attraction of Bi to Sn successfully induced a suitable upshift of the center of the outermost p orbitals of Sn, which not only weakened the Sn–C hybridization of \*COOH but also promoted the Sn–O hybridization of HCOO\* (Fig. 2e). Accordingly, the Sn–Bi catalyst achieved an improved formate partial current density of

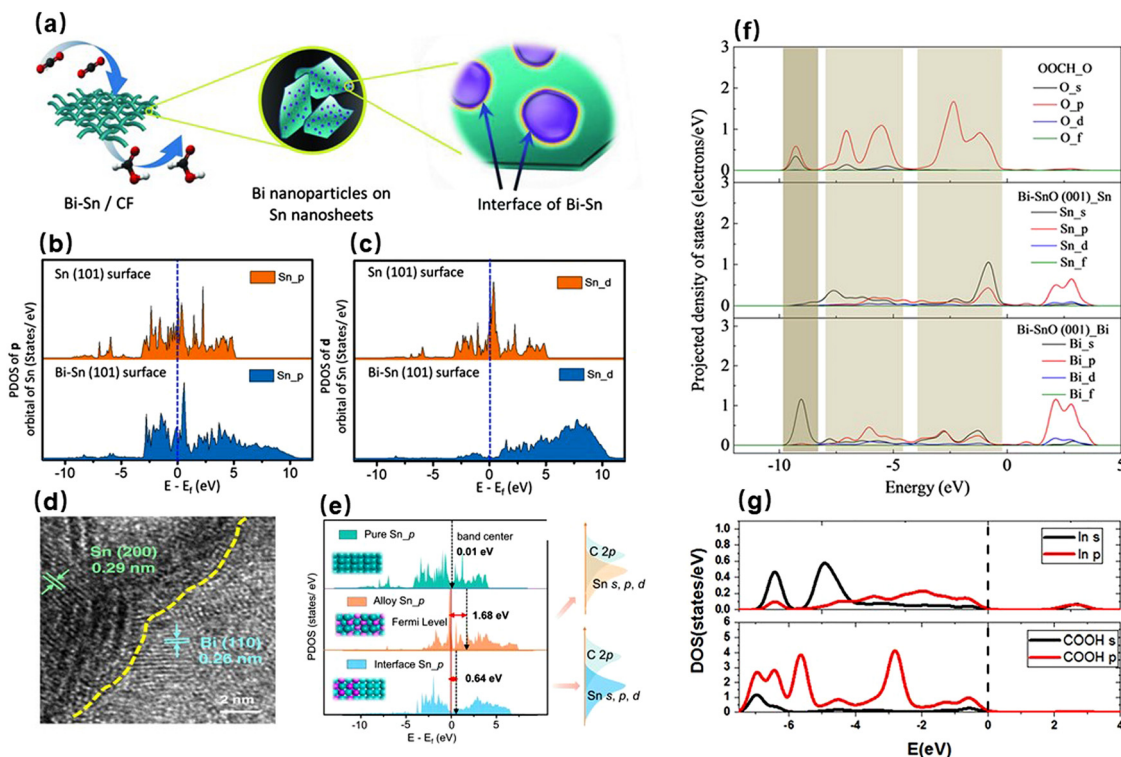


**Fig. 2** (a) Schematic diagram of Bi–Sn formed on a porous carbon matrix and an interface obtained by the deposition of Bi nanoparticles on Sn nanosheets. PDOS (projected density of states) of (b) p orbital and (c) d orbital of Sn atoms on the surfaces of Bi–Sn and Sn without  $\text{HCOO}^*$ .<sup>83</sup> Reproduced with permission from Wiley-VCH Verlag GmbH & Co. KGaA, copyright 2018. (d) High-resolution transmission electron microscopy (HRTEM) image of the nano-crumpled. (e) PDOS of the Sn 5p orbitals of alloy Sn, interface Sn, and pure Sn, and weighted band centers of the models without adsorbate, a scheme (right) for PDOS overlapping areas of the s, p, and d orbitals of Sn on the Sn–Bi bimetallic and Sn–Bi alloy interfaces with the C 2p orbitals of  $\text{*COOH}$ .<sup>84</sup> Reproduced with permission from Springer Nature, copyright 2022. (f) Bi–SnO(001) surfaces with adsorbed  $\text{*OOCH}$ .<sup>80</sup> Reproduced with permission from American Chemical Society, copyright 2019. (g) Density of states of  $\text{*COOH}$  on In-doped  $\text{Bi}_2\text{O}_3(010)$ .<sup>89</sup> Reproduced with permission from Elsevier, copyright 2022.

$140 \text{ mA cm}^{-2}$ . Tang *et al.* adopted a liquid-phase ultrasonication technique to synthesize a Bi–Sn nano-alloy.<sup>85</sup> Benefiting from the close contact between Bi and Sn, the highly electronegative Bi atoms drove the p and d orbitals of Sn atoms to undergo an upshift out of the Fermi level. This effect promoted the adsorption of active sites to reactants as well as the electron transfer between the two, thus enabling the catalyst to exhibit the enhanced performance. Wu *et al.* employed an aerogel method to prepare a Sn@Bi bimetallic catalyst, which showed a better selectivity for formate than pure Bi and Sn.<sup>86</sup> Because the strong hybridization between the p orbitals of Sn and Bi atoms increased the density of states of Sn@Bi(012) planes across the Fermi level, the resulting highly active Sn@Bi(012) planes showed the markedly reduced energy barrier for the generation of formic acid.

p-Block metal oxides are also catalytically active for the  $\text{CO}_2\text{RR}$ . However, the reduction potentials required to generate formate/formic acid are far more negative than the standard potentials for the p-block metal oxides, leading to their poor electrochemical stabilities.<sup>79</sup> On the other hand, modulating the electronic structures of p-block metal species can not only stabilize the valence states of p-block metal oxides in the operating environment but also further optimize their

adsorption strengths for reactants. For instance, An *et al.* introduced metallic Bi into SnO nanosheets by using a hydrothermal method to enhance the electrocatalytic activity.<sup>80</sup> They found that the doped Bi element successfully stabilized the divalent Sn ( $\text{Sn}^{2+}$ ), preventing it from being reduced to metallic Sn ( $\text{Sn}^0$ ) in the electrocatalytic  $\text{CO}_2\text{RR}$  process. In addition, the 6s orbital of Bi was hybridized with the O 2s and 2p orbitals (Fig. 2f). The orbital hybridization strengthened the adsorption capability of SnO surfaces toward  $\text{CO}_2$  and  $\text{HCOO}^*$ , which thereby promoted the formation of formic acid. Wu *et al.* also found that Sn–Bi bimetallic catalysts could lower the energy barrier for  $\text{*OOCH}$  and promote the production of  $\text{HCOOH}$ .<sup>87</sup> Wang *et al.* employed a wet-chemical method to prepare Sn–In alloy nanoparticles, consisting of an  $\text{InSn}_4$  core and an In-doped  $\text{SnO}_2$  shell.<sup>88</sup> The element indium in the  $\text{SnO}_2$  shell led to the generation of O vacancies, which not only stabilized the structure of  $\text{SnO}_2$  but also reduced the formation energy of  $\text{HCOO}^*$  on the surface of  $\text{SnO}_2$ . Moreover, the metallic  $\text{InSn}_4$  core inside the nanoparticle have the material high electrical conductivity. Consequently, the unique core–shell structure enabled the Sn–In alloy to obtain a current density of  $236 \text{ mA cm}^{-2}$  at  $-0.98 \text{ V}$  and a formate selectivity of 94% in a flow cell. Guan *et al.* utilized In to improve the electrocatalytic stability and activity

of  $\text{Bi}_2\text{O}_3$ .<sup>89</sup> The electrochemical performance and crystal phase of the In- $\text{Bi}_2\text{O}_3$  catalyst did not change during the 15 hour potentiostatic measurement, indicating its excellent stability. Moreover, the hybridization of the 5s and 5p orbitals of In with the 2s and 2p orbitals of  $\text{HCOO}^*$  promoted the formation of strong binding states between In and  $\text{HCOO}^*$ , which significantly reduced the free energy required for the generation of  $\text{HCOO}^*$  and hence boosted the generation of formic acid (Fig. 2g). According to Liu *et al.*, the S-modulated copper nanosheet also contributed to improved formate production from  $\text{CO}_2$ , maintaining a selectivity of 89.8% at an ultrahigh formate current density of  $404.1 \text{ mA cm}^{-2}$ .<sup>90</sup>

### 2.3 d-Block metals

d-Block metals (*i.e.*, transition metals) are a class of metals in which the last electron is filled into the d orbitals. They have relatively more valence electrons, allowing them to possess a variety of stable electron configurations.<sup>91</sup> Because the outermost d orbitals of d-block metals are easily hybridized with the C 2p orbitals, they tend to adsorb  $\text{CO}_2$  molecules in the form of carbon coordination during the electrocatalytic  $\text{CO}_2\text{RR}$  processes.<sup>92</sup> Therefore, the d-block metal active sites are conducive to converting  $\text{CO}_2$  into the  $^*\text{COOH}$  intermediate, which is subsequently transformed into CO after gaining an additional electron and proton.<sup>93–95</sup> If the adsorption strength of active sites to CO is relatively weak, CO will easily desorb from the active sites and become the main reduction product.<sup>96,97</sup> On the other hand, if the active sites stably adsorb CO, then CO can continue to undergo the proton-coupled electron transfer (PCET) reaction on the active sites and be converted into some deep-reduction products as exemplified by methane, ethylene, ethanol, *etc.*<sup>98–100</sup>

The electronic structures of transition metals are crucial for their electrocatalytic  $\text{CO}_2\text{RR}$  performances. For example, the metallic states of the first-row transition metals (*e.g.* Fe, Co, Ni, and Zn) have high activation energy barriers for  $\text{CO}_2$  molecules, enabling them to be more inclined to activate protons.<sup>101,102</sup> Especially for the metallic Zn, its fully occupied 3d orbital hinders electron transfer and reduces its catalytic activity for the  $\text{CO}_2\text{RR}$ . Interestingly, converting the metallic Zn to the low-valence  $\text{Zn}^{\delta+}$  ( $0 < \delta < 2$ ) could significantly enhance its  $\text{CO}_2\text{RR}$  performance, because unsaturated Zn sites had more spaces to couple  $\text{CO}_2$ /intermediates.<sup>103</sup> Density functional theory (DFT) calculation results demonstrated that Zn in the low-valence state could greatly reduce the reaction energy barrier of  $^*\text{COOH}$  (Fig. 3a and b). In addition, perturbing the originally stable electronic configurations of Zn atoms resulted in enhancing the activity of electrons in their 3d orbitals, which in turn allowed more electrons to participate in the stabilization of  $^*\text{COOH}$  (Fig. 3c). Accordingly, the low-valence Zn sites showed a higher CO selectivity than the saturated Zn sites in terms of the  $\text{CO}_2\text{RR}$ . Yang *et al.* found that electrons from the 3d orbitals of oxidized Ni(I) could spontaneously delocalize and enter the C 2p orbitals of  $\text{CO}_2$  molecules, which greatly boosted the adsorption of  $\text{CO}_2$  and intermediate species at the electrocatalyst surfaces.<sup>92</sup> The CO selectivity of monovalent Ni(I) active sites

could reach 97%, while that of metallic Ni was only about 75% (Fig. 3d and e). A negative shift in the valence band edge and a sharp decrease in the electron density of Ni 3d orbitals indicate the transfer of electrons from  $3dx^2-y^2$  of Ni(I) to  $2\pi_u$  of C, as exhibited in Fig. 3f and g, after the formation of  $\text{CO}_2^{\delta-}$  species on the surface of the catalyst A-Ni-NG.<sup>92</sup> Although the metallic states of the first-row transition metals have relatively poor catalytic activities toward the  $\text{CO}_2\text{RR}$ , modulating their valence states enables them to catalyze the reduction of  $\text{CO}_2$  into CO efficiently because the electrons of unfilled d orbitals of the low-valence metal sites are quite active. These d orbitals can easily hybridize the electronic orbitals of intermediates and thereby stabilize the species.

Noble metals in the second and third rows, such as Pd, Ag, and Au, also tend to generate CO because of their small CO desorption energies.<sup>104,105</sup> Nevertheless, the slow activation rates of  $\text{CO}_2$  molecules as well as the weak adsorptions of  $^*\text{COOH}$  on these metals require additional modulations toward their electronic structures to ensure an accepted level of activity and selectivity. As such, Zhu *et al.* adopted a self-assembly strategy to prepare Pd-Au bimetallic nanowires comprising the Pd-Au core and the pure Pd shell.<sup>106</sup> The doping of Au atoms into Pd lattices did change the local electronic properties and the d-band centers of Pd atoms, which greatly lowered the activation energy barrier of  $\text{CO}_2$  molecules. Moreover, the synergistic effect between Au and Pd evidently promoted the adsorption of  $^*\text{COOH}$  on the Pd/PdAu(110) facet. Thus, compared with the pure Pd nanoparticles, the electrocatalytic activity and selectivity of Au-modified Pd nanowires were significantly enhanced. Ozden *et al.* utilized Au adparticles to modulate the lattice and electronic structures of Ag, which allowed the electrocatalyst to efficiently convert  $\text{CO}_2$  to CO at low overpotentials.<sup>107</sup> Since the strongly electronegative Au drove the electrons in the Ag 3d orbitals to move to the high energy levels outside the nuclei, the resulting highly active Ag sites significantly reduced the free energy required to form  $^*\text{COOH}$ . In addition, the two adjacent sites of Au and Ag could simultaneously adsorb different atoms in one  $^*\text{COOH}$ , which significantly enhanced the adsorption strength of  $^*\text{COOH}$  at the electrocatalyst surface. The above studies have demonstrated that the electronic structural modulation of noble metals is able to decrease the activation energy barrier of  $\text{CO}_2$  molecules through strengthening the activity of outer electrons from host metals. Moreover, the synergistic adsorption of dual metals toward the key intermediate can greatly promote the efficient conversion of  $^*\text{COOH}$  to CO.

Since adsorption strengths to CO by the first-row transition metals such as Zn and Ni or noble metals such as Ag and Au are weak, it is easy for CO to desorb from active sites. In contrast, Cu has a moderate adsorption energy for CO, which enables this d-block element to continue transforming CO into deep-reduction products.<sup>61,100,108</sup> However, because the low activity of metallic Cu often results in small current densities, alongside poor product selectivities, it is necessary to modify the electronic configuration of Cu.<sup>109</sup> Modulating the electronic structures of Cu species can not only optimize the adsorption of

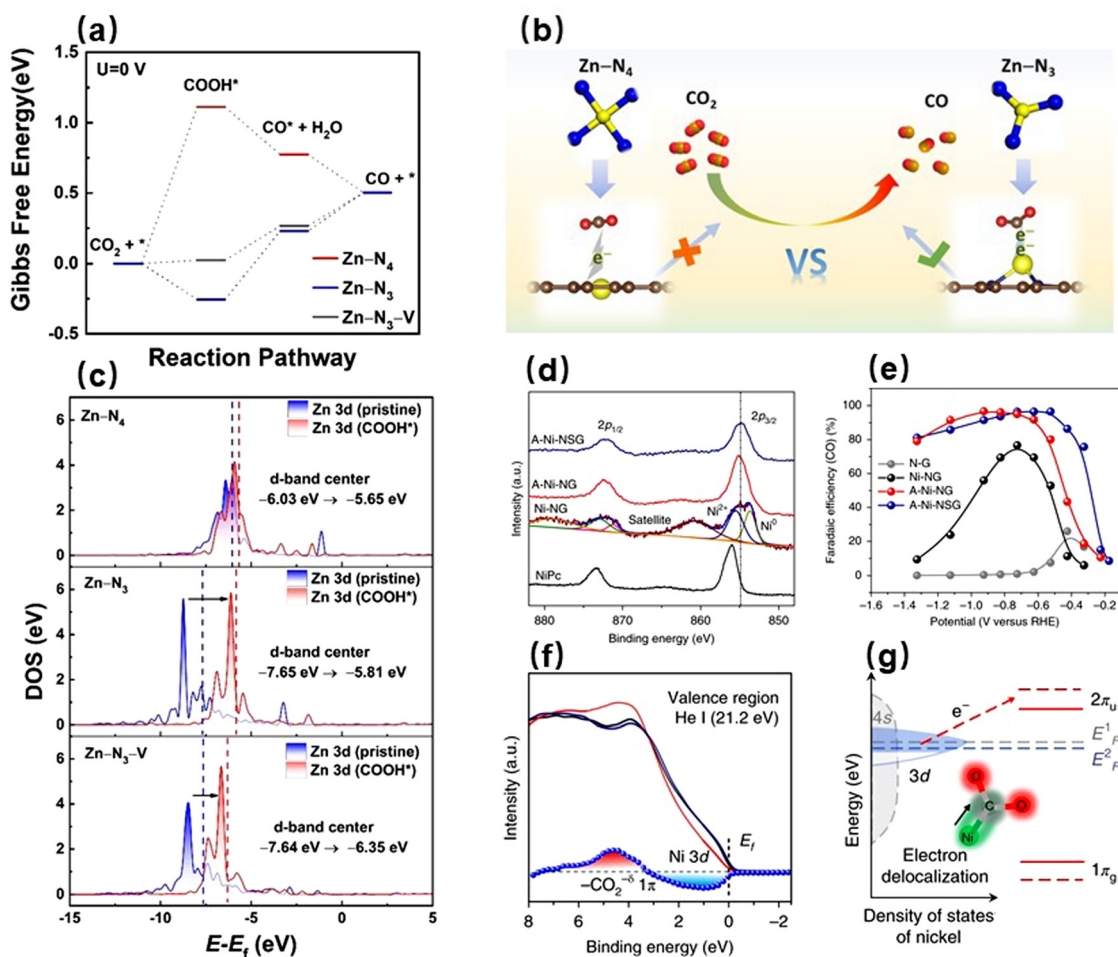


Fig. 3 (a) Gibbs free energy for the conversion of CO<sub>2</sub> to CO based on the graphitic Zn-N<sub>3</sub>-V, Zn-N<sub>3</sub> and Zn-N<sub>4</sub> models. (b) Comparison of active sites between Zn-N<sub>3</sub> and Zn-N<sub>4</sub>. (c) PDOS of the Zn-N<sub>3</sub>-V, Zn-N<sub>3</sub>, and Zn-N<sub>4</sub> models before and after the \*COOH interaction.<sup>103</sup> Reproduced with permission from Wiley-VCH Verlag GmbH & Co. KGaA, copyright 2021. (d) X-ray photoelectron spectroscopy (XPS) high-resolution Ni 2p spectra. (e) Faradaic efficiency of CO at various applied potentials. (f) Valence band spectra of A-Ni-NG before (black) and after (red) the CO<sub>2</sub> exposure, and after the desorption of CO<sub>2</sub> by thermal processing in vacuum for twenty minutes at 500 °C (dark blue). (g) Activation routes of CO<sub>2</sub> on the Ni(l) site.<sup>92</sup> With permission from Springer Nature, copyright 2018.

CO at Cu-related sites, promoting the CO protonation or the CO-CO coupling, but also enhance the binding strengths of these sites toward key intermediates in terms of a certain deep-reduction product, thus achieving high selectivity. For example, Cu<sub>2</sub>O with monovalent Cu(I) showed high methane selectivity in the CO<sub>2</sub>RR, because it could readily protonate CO to CHO\* (the key intermediate for the production of methane). At the same time, Cu<sub>2</sub>O also had high adsorption strengths for other intermediates in the methane pathway, such as CH<sub>2</sub>O\* and OCH<sub>3</sub>\*, thereby avoiding the formation of other by-products.<sup>98</sup> Yi *et al.* used a facile electroreduction process to synthesize Cu<sub>2</sub>O single-type sites, which showed an enhanced methane selectivity of 73% at -1.4 V.<sup>98</sup> The theoretical calculation results demonstrated that the energy barrier for the protonation of CO to CHO\* on the Cu<sub>2</sub>O(111) facet was only 0.43 eV. In addition, the PCET processes required the conversion of CHO\* to methane to be exothermic, which greatly promoted the formation of methane. Deng *et al.* prepared Cu<sub>2</sub>O microparticles

using an electrochemical reconstitution method, and they systematically studied the free energy changes ( $\Delta G$ ) of CO to CHO\* and CO to OCCOH\* on the Cu<sub>2</sub>O surfaces.<sup>110</sup> Notably, the  $\Delta G_{\text{CO} \rightarrow \text{CHO}^*}$  values were much smaller than  $\Delta G_{\text{CO} \rightarrow \text{OCCOH}^*}$  on Cu<sub>2</sub>O with different facets, reflecting the high affinity of Cu<sub>2</sub>O for CHO\*. Accordingly, the Cu<sub>2</sub>O surfaces with different facets all showed the high selectivities to methane. When other valence Cu species (such as CuO) were present in the Cu<sub>2</sub>O system, the selectivity of methane was significantly reduced.<sup>111</sup> According to the above works, it can be found that the high selectivity of Cu<sub>2</sub>O for methane is not related to its exposed facets, but benefits from the unique electronic structure of its Cu species.

Employing a second metal to enhance the local electron density of metallic Cu can improve the selectivity for multi-carbon products, on the grounds that the high electron density is beneficial to the adsorption of a large amount of CO at the Cu sites and thus promoting the CO-CO coupling and the



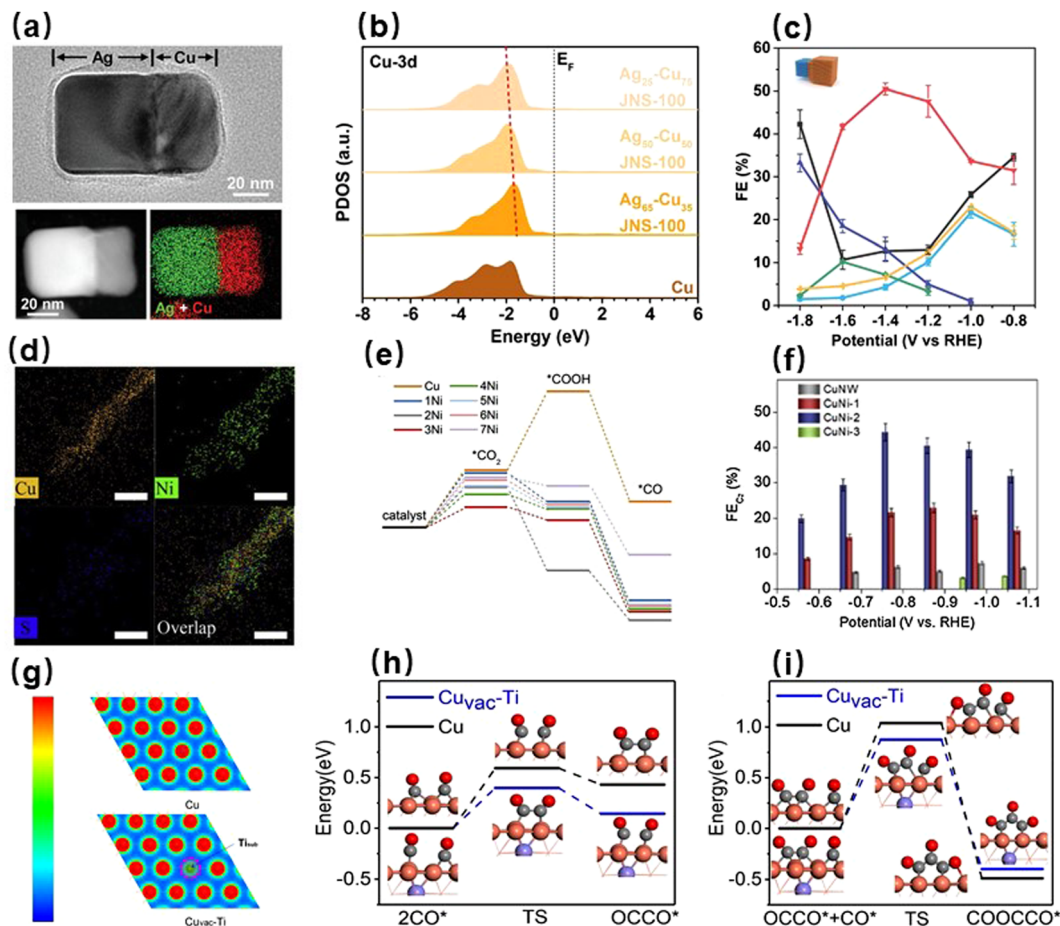


Fig. 4 (a) TEM and energy-dispersive X-ray spectroscopy (EDX) elemental mapping images of Ag<sub>65</sub>-Cu<sub>35</sub>. (b) PDOS comparison of Cu-3d. (c) FE of major CO<sub>2</sub>RR products formed by Ag<sub>65</sub>-Cu<sub>35</sub> JNS-100.<sup>112</sup> Reproduced with permission from Wiley-VCH Verlag GmbH & Co. KGaA, copyright 2022. (d) EDX elemental mapping images of Ni-CuNW. (e) Free energy for CO<sub>2</sub> activation by Ni-decorated Cu surfaces and pristine Cu(111). (f) FE comparison of C<sub>2+</sub> by Ni-CuNW and CuNW.<sup>113</sup> Reproduced with permission from Elsevier, copyright 2021. (g) Charge-density distributions of Cu<sub>vac</sub>-Ti and Cu. Free energy profiles of (h) dimerization and (i) trimerization of \*CO at the Cu<sub>vac</sub>-Ti and Cu sites.<sup>114</sup> Reproduced with permission from Wiley-VCH Verlag GmbH & Co. KGaA, copyright 2021.

subsequent protonation. Furthermore, the optimization of density of states of Cu d orbitals near the Fermi level by the foreign metals can strengthen the activity of electrons in the d orbitals, thereby reducing the reaction energy barriers. For example, Ma *et al.* utilized confined growth of Cu on Ag nanocubes to synthesize Janus nanostructures of Ag-Cu with (100) facets (Fig. 4a).<sup>112</sup> Because the intimate electronic interaction between Cu and Ag induced the upshift of the centers of Cu 3d orbitals toward the Fermi level (Fig. 4b), the surface Cu sites exhibited a high electroactivity for the adsorption of OCCO\*. At the same time, the Ag 4d orbitals also presented this upshift, which facilitated the transfer of electrons from silver to copper and further to the adsorbates. In this way, the Ag-Cu catalyst displayed an enhanced C<sub>2+</sub> selectivity of 72% at -1.4 V (Fig. 4c). Zhang *et al.* developed a coordination enabled galvanic replacement approach to evenly distribute atomic Ni clusters over Cu surfaces that were rich in defects (Fig. 4d).<sup>113</sup> The appearance of Ni-Cu bridges allowed Cu atoms to acquire extra electrons from the adjacent Ni atoms, which increased the

local electron densities of Cu atoms. In addition, the intrinsically catalytic activity of Cu atoms was significantly enhanced, identified by the increased adsorption strength of CO and the decreased energy barrier of the CO-CO coupling on the Cu atoms (Fig. 4e). Thus, the highly active electrocatalyst CuNi-2 exhibited a seven-fold increase in the selectivity for C<sub>2+</sub> products compared to pristine Cu (Fig. 4f). Moreover, a Cu-Ti alloy was prepared through an etching dealloying process and used for electrocatalytic CO<sub>2</sub>RR toward multi-carbon (C<sub>2-4</sub>) liquid fuels.<sup>114</sup> As shown in Fig. 4g, the subsurface Ti atoms with the relatively low electron affinity could donate their electrons to the surface Cu atoms, and the resulting Cu active sites with high electron densities were able to both facilitate the adsorption of CO and reduce the activation energy barriers of dimerization and trimerization of CO (Fig. 4h and i). As a consequence, the Cu-Ti alloy yielded ethanol, acetone, and *n*-butanol as its major products. Different types of metals can be utilized to optimize the electronic structure of Cu to improve the catalytic selectivities for multi-carbon products. The precise

modulation of electronic structures can efficiently tune the intermediate coupling and protonation processes, thereby expanding the product diversity of electrocatalytic CO<sub>2</sub>RRs.

## 2.4 f-Block metals

f-Block lanthanoid metals with the last electron being filled into the f orbitals possess a strong lanthanide contraction effect due to their loose 4f and unfilled 5d orbitals, giving them the capability to modulate the local electronic structures of other metal species.<sup>115</sup> However, how to coordinately combine lanthanoids with other metals is a huge challenge due to their relatively large atomic radii. Fortunately, the Xu group successfully synthesized a Ni–Gd–N ternary doped carbon black catalyst through a two-step method of self-assembly and pyrolysis.<sup>116</sup> Uniformly dispersed Gd atoms modulated the local electronic structure of Ni(I) active sites exposed outside the carbon layers and tailored the size of Ni nanoparticles wrapped inside the carbon matrix (Fig. 5a). Specifically, the Gd atoms drove the electrons in the outermost Ni 3d orbitals to higher energy levels because of their remarkable electron-withdrawing capability, thereby enhancing the electronic activity of Ni(I) active sites (Fig. 5b). Moreover, the doping of Gd atoms into the lattices of Ni nanoparticles reduced the particle size of the latter, which was beneficial to inhibiting the tendency of the

hydrogen evolution reaction (HER) for the Ni nanoparticles. The incorporation of Gd modified the adsorption energy of \*COOH at the Ni(I) active sites from –1.2 to –1.6 eV, indicating the enhanced adsorption strength of this key intermediate (Fig. 5c). Thus, the Gd-modified Ni-based electrocatalyst exhibited a high CO selectivity of 97% along with a high current density of 308 mA cm<sup>–2</sup> at –0.91 V (Fig. 5d). After that, Feng *et al.* doped Gd atoms into copper catalysts to modulate the electronic structure of the latter and significantly enhanced the activity of CO<sub>2</sub>-to-C<sub>2+</sub> products.<sup>117</sup> Zhao *et al.* reported that the oxophilic metal (La) was able to modulate the catalytic activity of Cu, improving the CH<sub>4</sub> selectivity (up to 64.5%), which was approximately 7.8 times higher than for Cu.<sup>118</sup> Infrared spectroscopy and DFT theoretical calculations showed that the presence of La would lead to stronger \*CH<sub>x</sub>O adsorption and promote the cleavage of C–O for \*CH<sub>3</sub>O, thus increasing the proportion of CH<sub>4</sub> in the products.

Currently, utilizing the f-block metals to modulate the electron structures of other metal species is seldom reported. However, the unique f orbitals of lanthanoid metals can indeed give rise to the strong hybridization with outer orbitals of other metal species, allowing the f-block elements to easily modulate the electronic structures of the latter. Consequently, the f-block metals possess the broad development prospects in terms of electronic structure regulation.

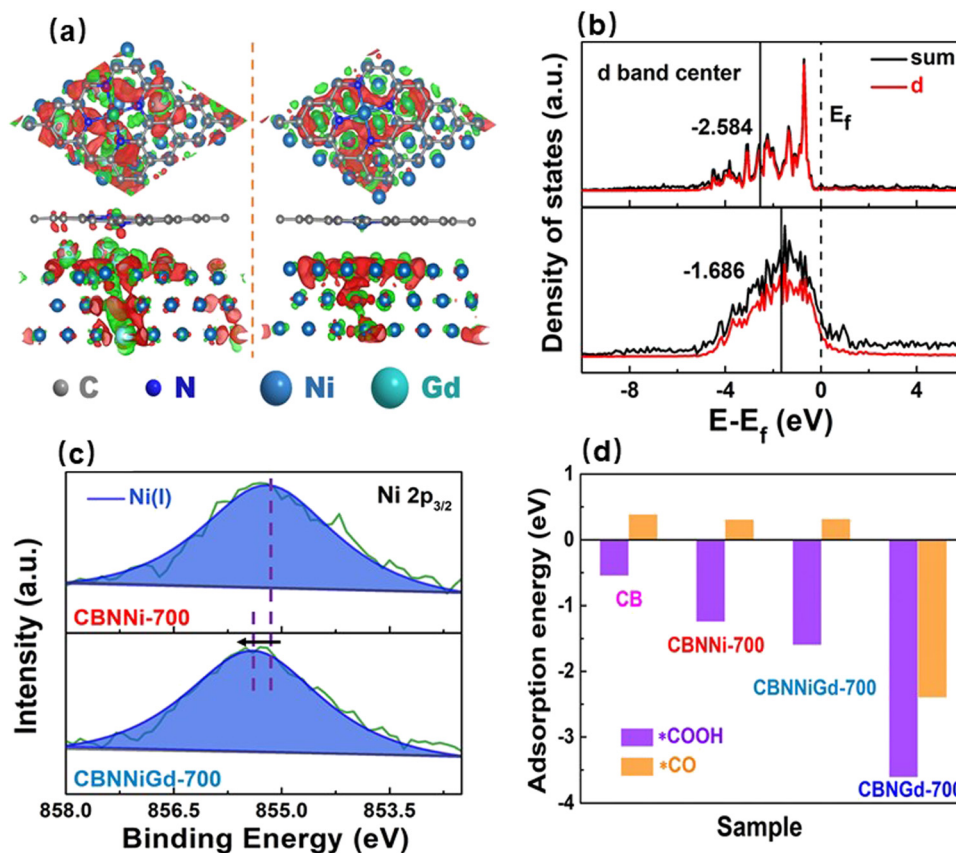


Fig. 5 (a) Charge-density redistributions of CBNNiGd-700 (left) and CBNNi-700 (right). (b) Total density of states (TDOS) and PDOS of Ni 3d and (c) XPS high-resolution Ni 2p<sub>3/2</sub> spectra of CBNNi-700 (upper) and CBNNiGd-700 (lower). (d) Adsorption energies of \*CO and \*COOH for various electrocatalysts.<sup>116</sup> Reproduced with permission from Wiley-VCH Verlag GmbH & Co. KGaA, copyright 2022.

From the above studies, the electronic structures of active sites of electrocatalysts play a crucial part in the CO<sub>2</sub>RR performance. As mentioned earlier, for instance, the p-block metal species tend to convert CO<sub>2</sub> to formate/formic acid, noble metals selectively generate CO, and Cu is able to generate deep-reduction products. It can therefore be summarized that the modulation of electronic structures of catalytically active sites could be achieved by introducing a second metal species ('guest') into host metals. The incorporation and doping of guest metal species into the host would give rise to a series of changes in the electronic configurations of active sites as well as the properties of the outermost orbital electrons, which can strengthen the orbital hybridization between electrocatalysts and CO<sub>2</sub>/intermediates and thereby improve their adsorption strengths. Since different atoms possess distinct electronic structures, certain combinations of atoms can lead to desired electronic structures, which means that atoms with appropriate electronic configurations can be selected and integrated *via* the precise modulation of electronic structures to achieve the required results of the CO<sub>2</sub>RR. It is noteworthy that electronic structural modulation is a highly sophisticated means of regulation, involving a set of microscopic processes such as electron delocalization and orbital hybridization. Therefore, a deep understanding of the underlying mechanisms of electronic structural modulation is necessary to prepare better electrocatalysts for CO<sub>2</sub>RRs.

### 3. Geometric structural modulation

In addition to electronic structures of metal species, geometric structures of catalyst supports can also exert considerable influence on CO<sub>2</sub>RR behaviors.<sup>45,56,57</sup> The Cu catalyst possessing a cavity structure exhibited an high current density and an outstanding FE for the reduction of CO<sub>2</sub> to C<sub>2+</sub> products as the cavity structure could increase the local concentration of CO.<sup>119</sup> Nevertheless, because metals can be directly used as current collectors and catalytically active sites for the CO<sub>2</sub>RR, they are prone to electrochemical corrosion and performance degradation.<sup>120</sup> Therefore, it is necessary to anchor metal species within geometric structures of corrosion-resistant supports.<sup>121,122</sup> In this way, catalyst supports can protect these metal species against agglomeration, migration, and loss during electrochemical reactions. Modulating the geometric structures of supports can not only increase pores and specific surface areas of electrocatalysts, providing increased attachment points for metal species, but also enhance the adsorption capacities for CO<sub>2</sub>/intermediates, supplying sufficient reaction-related molecules to metal species.<sup>123</sup> Moreover, some unique geometric structures of catalyst supports can exert their size effects, facilitating the efficient transfer of electrolyte, CO<sub>2</sub>/intermediate molecules, and products and thereby enhancing the electrocatalytic performance.<sup>56</sup> In this review, carbon supports are divided into three subcategories: synthetic carbon matrix, biomass matrix and coal matrix.

The synthetic carbon matrix provides a variety of options for electrocatalysts because of their controllable porous structures.

For instance, Li *et al.* prepared a hollow porous urchin-like microparticle carbon support anchored with Ni atoms (Fig. 6a and b), denoted as Ni-NC(HPU).<sup>124</sup> The two-sided available surfaces and the protruding nanothorns of the carbon support greatly increased the number of catalytically active sites and electrochemical surface areas. In addition, the abundant mesoporous structures of the urchin-like microparticles and the rich voids between them could effectively promote the adsorption and diffusion of CO<sub>2</sub> molecules, thereby achieving efficient mass transfer. To verify the advantages of the urchin-like geometric structure, they also prepared other hollow porous catalysts with similar components but different geometric structures, including wire-like and sphere-like geometric structures. Electrochemical measurements showed that Ni-NC(HPU) had similar CO selectivity to the two control samples, but the current density of Ni-NC(HPU) was much higher (Fig. 6c). These results demonstrated that modulating the geometric structure of the catalyst support *via* its size effect can significantly enhance the electrocatalytic activity. Additionally, the geometric structure of the support also plays a major role in the electrochemical performance of metal-free catalysts.<sup>125-127</sup> Because modulating the geometric structures of supports can optimize the local properties of materials, the resulting favorable microenvironments in the supports become conducive to enhancing the electrocatalytic performance of nonmetallic active sites. Ni *et al.* prepared a cage-like porous carbon doped with fluorine (F-CPC) through the template approach (Fig. 6d).<sup>128</sup> The cage-like carbon support with abundant micropores and moderate mesopores facilitated the capture and diffusion of CO<sub>2</sub> molecules, conducive to the improvement in mass transfer. More importantly, these opening circular pores on the support surface could accumulate charges, thus enhancing the local electric field intensity within the porous domains. The locally enhanced electrostatic field in the catalyst support was able to accumulate surface-adsorbed K<sup>+</sup> ions (Fig. 6e), which not only promoted the rapid stabilization of CO<sub>2</sub> molecules on the F sites but also reduced the energy barrier. And the current density of F-CPC was significantly higher than that of undoped catalysts (Fig. 6f). Therefore, F-CPC showed a considerable current density of 37.5 mA cm<sup>-2</sup> and a high CO selectivity of 88.3% at -1.0 V. In contrast, the CO selectivity of the control sample obtained by directly incorporating F into commercial carbon black could reach 90%, but its maximum current density was as low as 0.3 mA cm<sup>-2</sup>.<sup>129</sup>

Aside from the synthetic carbon matrix, renewable biomass is a high-performance carbon source and support. As a natural support, biomass is often employed as a catalyst precursor due to its unique porous structure. Li *et al.* prepared nitrogen-doped biochar with high surface area and hierarchical porosity by the carbonization of wheat flour using KOH, achieving CO selectivity of 83.7% at -0.82 V (Fig. 6g and h).<sup>130</sup> In a similar way, Yao *et al.* regulated the carbonization conditions of Typha to obtain nanoporous nitrogen-doped carbon with a high surface area and electric conductivity, which presented high CO selectivity (90%) at -0.31 V.<sup>131</sup> Moreover, a biomass-based electrocatalyst with a specific surface area of 1673.6 m<sup>2</sup> g<sup>-1</sup>

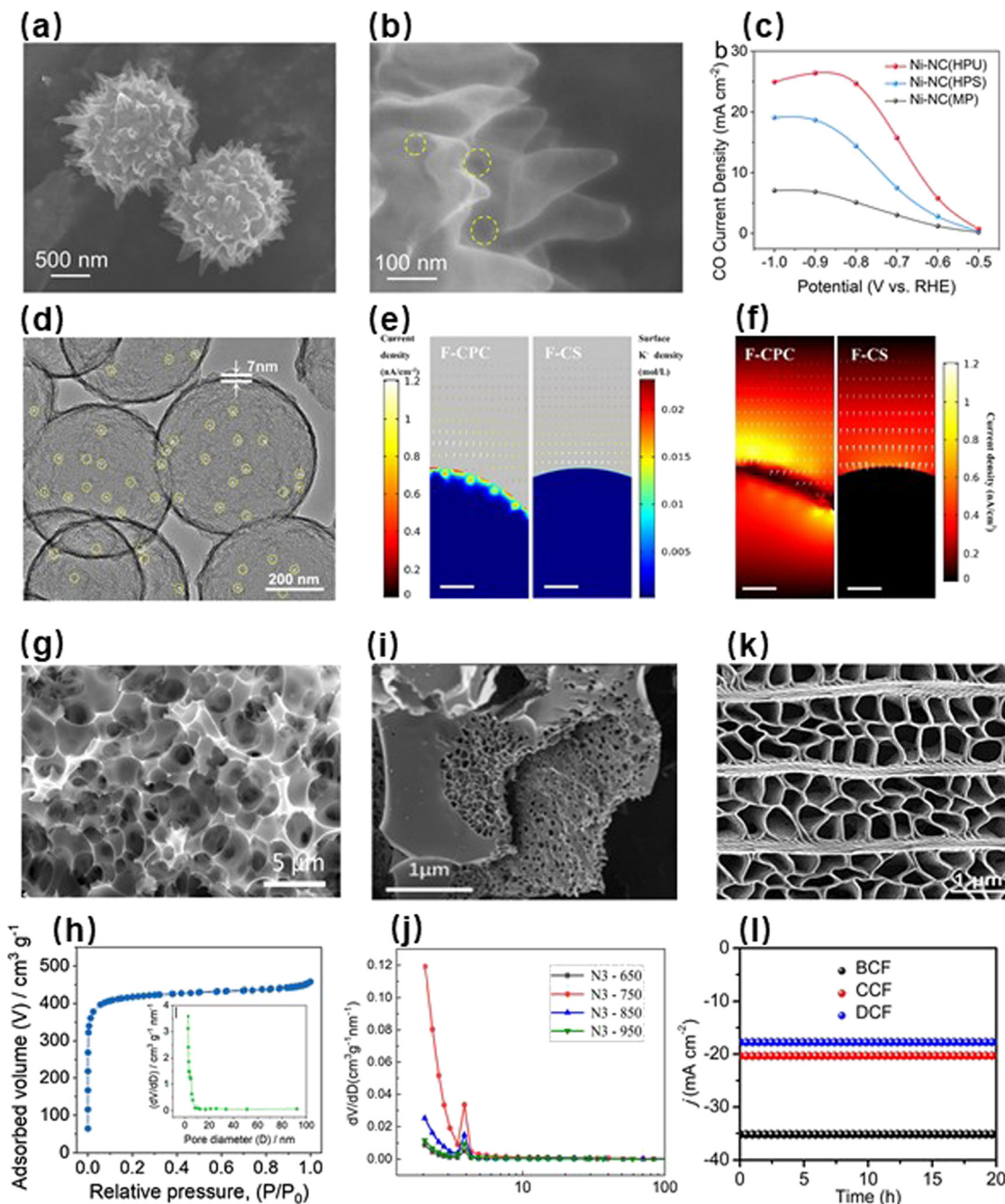


**Fig. 6** (a and b) Field-emission scanning electron microscopy (FESEM) images of Ni-NC(HPU). (c) CO partial current density of the electrocatalysts at various potentials.<sup>124</sup> Reproduced with permission from Wiley-VCH Verlag GmbH & Co. KGaA, copyright 2022. (d) TEM image of F-CPC. (e) Current-density distributions and surface K<sup>+</sup>-ion concentrations of F-CS and F-CPC. (f) Current-density distributions of F-CS and F-CPC in terms of the CO<sub>2</sub>RR.<sup>128</sup> Reproduced with permission from American Chemical Society, copyright 2020. (g) SEM image of NDC-700. (h) N<sub>2</sub> adsorption–desorption isotherms and pore size distribution (inset) for NDC-700.<sup>130</sup> Reproduced with permission from Elsevier, copyright 2017. (i) SEM image of N3-850.<sup>133</sup> With permission from Elsevier, copyright 2023. (k) SEM image of BCF. (l) Chronoamperometric results of the catalysts at –0.9 V.<sup>135</sup> Reproduced with permission from Springer Nature, copyright 2021.

was also prepared by using cedar as the carbon source, with the CO selectivity of 91% at low potentials.<sup>132</sup> As a common biomass material, the carbon aerogel derived from cellulose exhibited a large specific surface area, and its pore size distribution was quite uniform, within the range between 1 and 3 nm (Fig. 6i and j), providing good transfer channels for CO<sub>2</sub>

and its products.<sup>133</sup> Chen *et al.* mixed an N-rich silkworm cocoon with ZnCl<sub>2</sub> and then pyrolyzed them to acquire the biochar with abundant intrinsic defects.<sup>134</sup> Some of the N-containing groups in the biomass carbon matrix were removed during the pyrolysis process, resulting in vacancy defects and greatly improving the electrocatalytic CO<sub>2</sub>RR behaviors.

Using insect wings as precursors, Qi *et al.* synthesized a porous electrocatalyst with excellent electrochemical performance *via* pyrolysis processing at high temperatures (Fig. 6k).<sup>135</sup> As shown in Fig. 6l, the abundant ordered pores gave these biomass-based electrocatalysts with high current densities. According to the above works, modulating the geometric structures of catalyst supports, derived from either synthetic carbon matrix or biomass matrix, can effectively promote the adsorption and conversion of CO<sub>2</sub> molecules and therefore optimize the electrocatalytic CO<sub>2</sub>RR performance from both kinetic and thermodynamic aspects.

The carbon supports mentioned above were all prepared by calcining organic precursors, which inevitably caused some heteroatoms to be wrapped deep inside the supports. These deeply buried heteroatoms not only fail to play a catalytic role but also limit the overall activities of electrocatalysts.<sup>94</sup> In view of this, the Xu group have focused on natural carbon materials and found that coal has great application potential as the high-quality carbon support.<sup>136–139</sup> The robust carbon frameworks of coal enable the activation and doping treatments to introduce porous structures and heteroatoms only on the surface layers of coal particles, which can fully expose active sites and effectively guarantee the stability of catalysts. In addition, modulating the porous structures of coal-based supports can intensify the electron/substrate interaction, which significantly improved the electrocatalytic activity. As such, the Xu group prepared

N-doped porous coal catalysts using the solvent evaporation induced self-assembly approach.<sup>136</sup> It can be seen from Fig. 7a that the surface layers of coal were modified by activation and doping during the high-temperature processing whereas the internal structures of coal particles were dense and remained intact. In other words, the internal robust framework of coal was retained (Fig. 7b and c). As shown in Fig. 7d, the high electrochemical surface area of NPC-900 showed that a great number of microporous structures and nitrogen sites could provide abundant reaction sites for the CO<sub>2</sub>RR. The elevated temperature-induced pore shrinkage effect resulted in the formation of a large amount of micropores on the surface layers of the coal support, and N atoms were firmly anchored in these micropores. The spatial confinement effect of micropores in the coal support made the N atoms in the pores generate strong polarization, which significantly promoted the charge transfer from N atoms to CO<sub>2</sub> molecules. Therefore, the coal-based electrocatalyst showed a small onset potential for the CO product (−0.16 V), and its maximum CO selectivity could reach 95% at −0.67 V. On the basis of this work, the Xu group co-anchored a transition metal Ni and a non-metal N to micropores of robust coal-based carbon support (CNNi-700) by the self-assembly strategy to further enhance the electrocatalytic CO<sub>2</sub>RR performance.<sup>137</sup> The physicochemical characterization data revealed that the spatial confinement growth effect in the coal support gave rise to the immobilization of

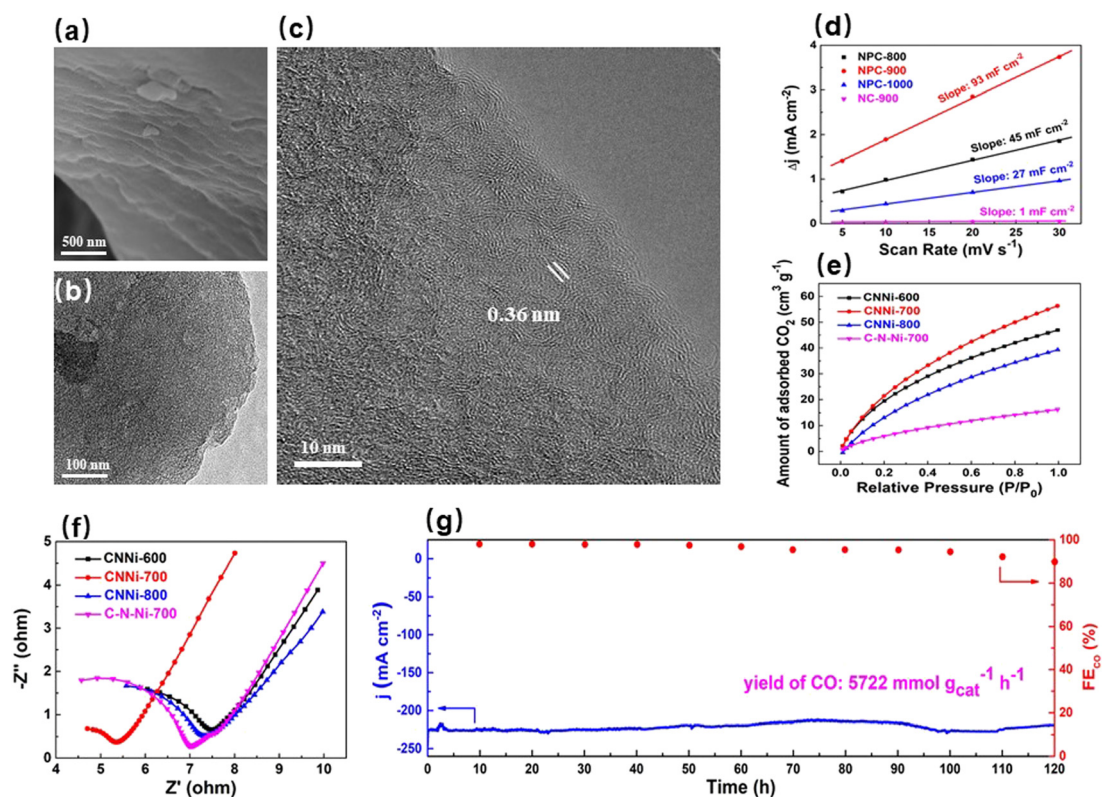


Fig. 7 (a) FESEM and (b and c) TEM images of NPC-900. (d) Dependence of charging current density differences on scan rates of the catalysts.<sup>136</sup> Reproduced with permission from Elsevier, copyright 2020. (e) CO<sub>2</sub> adsorption isotherms of the catalysts. (f) Nyquist plots of the catalysts. (g) Long-term stability test of CNNi-700 at −0.93 V in a flow cell.<sup>137</sup> Reproduced with permission from Elsevier, copyright 2021.

Ni–N active sites in the micropores, which could effectively inhibit the agglomeration of Ni species and increase the number of active sites. Additionally, these abundant microporous structures significantly elevated the CO<sub>2</sub> capacity of CNNi-700, which efficiently supplied CO<sub>2</sub> to the active sites, thus providing ample reaction substrates for the Ni–N active sites anchored within the micropores (Fig. 7e). Electrochemical tests showed that the coal support possessed a lower charge-transfer resistance than the organic precursor-derived carbon support, indicating the higher conductivity of the former (Fig. 7f). Thus, the highly efficient interaction between electron and substrate at the Ni–N active sites enabled CNNi-700 to maintain a CO selectivity of greater than 90% over a wide potential range, and its maximum CO selectivity and partial current density could reach 97% and 223 mA cm<sup>-2</sup>, respectively, as shown in Fig. 7g. It is noteworthy that the electrocatalytic CO<sub>2</sub>RR activity of CNNi-700 remained stable within a long-term potentiostatic measurement for 120 h, reflecting its outstanding stability and great potential for industrial application.

It can be summarized from the above-mentioned discussion that modulating the geometric structures of carbon supports derived from coal, biomass, and synthetic carbon matrixes is important for improving the adsorption capacities of electrocatalysts for substrates and promoting the size effect of support structures to facilitate the CO<sub>2</sub>RR performance. The porous structures and heteroatom distributions of biomass or synthesized carbon supports prove to be ubiquitous and uniform. Despite the fact that they are capable of obtaining good catalytic activities, their soft structures can also lead to a large number of heteroatoms being trapped within the internal materials, unable to exert their intrinsically catalytic capabilities. In contrast, the geometric structures of coal-based supports are so dense that doping treatments can allow extrinsic heteroatoms to be only doped and distributed on the surfaces, which to a large extent exposes the catalytically active sites and enhances the catalyst utilization. It is worth mentioning that the robust carbon skeletons inside the coal-based supports can provide strong support and protection for active sites, not only enabling the electrocatalysts to achieve high selectivities and large current densities in wide potential windows but also

significantly improving the long-term catalytic stabilities. Whether it is biomass or coal, the exploration of natural carbon materials as catalyst supports can decrease the usage of organic reagents and reduce the production cost of electrocatalysts, which also proves to be environmentally friendly and conducive to the industrialization of the CO<sub>2</sub>RR. The representative CO<sub>2</sub>RR electrocatalysts whose geometric structures were modulated are summarized in Table 2.

## 4. Conclusions and outlook

The utilization of renewable energy for electrochemical conversions of CO<sub>2</sub> to high-value-added chemicals presents a highly promising research area for sustainable development. As the electronic structures of active sites and the geometric structures of supports are the two critical factors that influence the performance of CO<sub>2</sub>RR electrocatalysts, this review summarizes the recent research progress of enhancing the catalytic activities and selectivities through electronic and geometric structural modulation strategies, and systematically analyzes the impacts of these two strategies on catalyst performance and structure–activity relationships. Despite the significant progress made regarding the electronic and geometric structural modulations of CO<sub>2</sub>RR electrocatalysts in recent years, there are still many important areas of research that are primitive or unclear. For example, roles of lanthanoid metals in electrocatalytic behaviors are yet to be well understood; heteroatoms can hardly be doped precisely to the desired sites; there are still unsolved issues in the utilization of staple carbon sources from nature; the combined effects of electronic and geometrical modulations need to be deeply explored; and the complexities of electrochemical interfaces and electrocatalytic conversions make calculations and modelling quite challenging. Our suggestions can now be summarized as follows:

(1) Using f-block lanthanoid elements. The strong spin–orbit coupling effect induced by the unique electronic configurations of f-block lanthanoids can be utilized for enhancing the performance of CO<sub>2</sub>RR electrocatalysts. Doping lanthanoid elements into the host metal is indeed an effective way to

**Table 2** Summary of representative CO<sub>2</sub>RR electrocatalysts whose geometric structures were modulated

| Matrix           | Product | Electrocatalyst        | Reactor     | Electrolyte             | FE (%) | <i>j</i> (mA cm <sup>-2</sup> ) | <i>E</i> (V vs. RHE) | Ref. |
|------------------|---------|------------------------|-------------|-------------------------|--------|---------------------------------|----------------------|------|
| Synthetic carbon | CO      | A–Ni@CMK               | H-type cell | 0.5 M KHCO <sub>3</sub> | 95     | 51                              | –0.8                 | 56   |
|                  | CO      | C–Au-500               | H-type cell | 0.5 M KHCO <sub>3</sub> | 94     | 150                             | –0.35                | 120  |
|                  | CO      | Fe–N/CNT@GNR-2         | H-type cell | 0.1 M KHCO <sub>3</sub> | 98     | 12                              | –0.76                | 121  |
|                  | CO      | Ni–NC(HPU)             | H-type cell | 0.5 M KHCO <sub>3</sub> | 91     | 24.7                            | –0.8                 | 124  |
|                  | CO      | F–CPC                  | H-type cell | 0.5 M KHCO <sub>3</sub> | 88.3   | 37.5                            | –1.0                 | 128  |
|                  | CO      | NSHCF                  | H-type cell | 0.1 M KHCO <sub>3</sub> | 94     | 100                             | –0.7                 | 140  |
| Biomass          | CO      | CB–NGC-2               | H-type cell | 0.1 M KHCO <sub>3</sub> | 91     | 6.5                             | –0.76                | 141  |
|                  | CO      | COF@MOF800–Co          | H-type cell | 0.5 M KHCO <sub>3</sub> | 92.6   | 9                               | –0.8                 | 142  |
|                  | Formate | N–BiNSs                | H-type cell | 0.5 M KHCO <sub>3</sub> | 92.25  | 30                              | –0.95                | 143  |
|                  | CO      | PPy@MOF-545–Co         | H-type cell | 0.1 M KHCO <sub>3</sub> | 98     | 10                              | –0.8                 | 144  |
|                  | CO      | AgNNs@Zn <sub>15</sub> | H-type cell | 0.5 M KHCO <sub>3</sub> | 91.05  | 6.5                             | –0.86                | 145  |
|                  | CO      | Fe–N–PC                | H-type cell | 0.5 M KHCO <sub>3</sub> | 90     | 11.44                           | –0.49                | 146  |
|                  | CO      | FeSA–S/N–C-9           | H-type cell | 0.5 M KHCO <sub>3</sub> | 96.3   | 4.9                             | –0.48                | 147  |
| Coal             | CO      | NPC-900                | H-type cell | 0.5 M KHCO <sub>3</sub> | 95     | 2.3                             | –0.67                | 136  |
|                  | CO      | CNNi-700               | Flow cell   | 1.0 M KOH               | 97     | 223                             | –0.93                | 137  |

regulate the electronic configurations of the host active species, which is conducive to accelerating electron transfer and optimizing the adsorption strengths of reactants/intermediates, thereby improving product selectivities. In addition, the large atomic radii of lanthanoid metals can cause lattice defects in the host active species if the f-block elements are successfully doped into the host. The decrease in crystallinity of the host metal is therefore beneficial for exposing large quantities of low-coordination high-activity sites, helping to further enhance electrocatalytic activities.

(2) Precisely regulating the doping states of heteroatoms. The doping level of heteroatoms, regardless of whether they are metals or nonmetals, is an important parameter for modulating the electronic structures of active sites of CO<sub>2</sub>RR electrocatalysts. Generally speaking, the more the doping level, the greater the change in the intrinsically electronic structures of active sites. However, as far as the catalytic performance is concerned, the doping level of heteroatoms is not necessarily the more the better. The optimal catalytic behaviors may only require a small but suitable quantity of heteroatoms to tune the electronic structures. Thus, how to precisely regulate the doping level and how to accurately dope specific heteroatoms into correct sites are very challenging problems that need to be solved urgently, because they directly affect the electrocatalytic performance.

(3) Exploiting natural carbon sources as catalyst supports. As mentioned earlier, geometric structures of catalyst supports play an indispensable role in the CO<sub>2</sub>RR performance. Carbon supports derived from natural materials, particularly biomass and coal, are worthy of attention. The geometric structures of biomass, which are naturally formed and difficult to synthesize artificially, provide excellent channels for mass and charge transfers as well as favorable distribution space for catalytically active sites. The diverse geometric structures of biomass include but are not limited to vascular bundle structures, hierarchical pores, wrinkled rough textures, and loose spongy porous structures. These natural structures provide excellent platforms for electrocatalytic reactions without the need for complex and cumbersome artificial construction, which also lay an important foundation for further modification and optimization. In addition, coal, which is formed by long-term geological processes from biomass, possesses robust structures that make it an excellent candidate for addressing the stability problem of electrocatalysts working in electrochemical environments. Meanwhile, the microporous structures of coal can give rise to the spatial confinement effect that promotes electrocatalytic reactions, which has great scientific research values and exploration space. It is worth noting that biomass and coal, as widely available natural carbon materials, still have countless unique geometric structures that are yet to be discovered or utilized. As rich natural treasures, they urgently need to be explored by researchers.

(4) Combining electronic modulation with geometric modulation. The modulations of both electronic and geometric structures give rise to the performance enhancement of CO<sub>2</sub>RR electrocatalysts. Thus, a synergistic combination of electronic and geometric structural modulations of electrocatalysts

should pave promising avenues for promoting the CO<sub>2</sub>RR performance, by optimizing the electrocatalytic CO<sub>2</sub>RR processes through the geometric structural modulation of catalyst supports to provide abundant active sites and facilitate mass transfer, and also by optimizing the electronic structural modulation of active sites to improve the adsorption of CO<sub>2</sub>/intermediates. To acquire a high-performance electrocatalyst that is both highly catalytically active and stable, there are still many research gaps that need to be filled. Indeed, interdisciplinary research in physics, chemistry, biology, materials science, and other related fields will undoubtedly be a promising approach to achieve the research goals.

(5) Pushing the limits for calculations and modelling. Finding suitable descriptors that can accurately reflect the structure–performance relationship in terms of electrocatalytic CO<sub>2</sub>RR is key to high-throughput screening of potential catalysts. Due to the enormous computational workload, it is necessary to utilize artificial intelligence (AI) technologies as exemplified by machine learning. Of course, the basis is to establish complete databases of catalysts. Furthermore, calculation methods that can efficiently and accurately obtain electronic structures need to be further developed, together with advanced approaches to modelling electrochemical interfaces based on density functional theory molecular dynamics (DFTMD). In short, a truly deeper understanding of fundamentals and mechanisms of the electronic and geometric modulations for optimizing the CO<sub>2</sub>RR requires continuous improvement and crossover between experimental, theoretical, and computational research studies.

## Conflicts of interest

There are no conflicts to declare.

## Acknowledgements

This study was financially supported by the National Key Research and Development Program of China (2021YFB4001502), the National Natural Science Foundation of China (51702358), the Natural Science Foundation of Jiangsu Province (BK20170281), and the Fundamental Research Funds for the Central Universities (2019ZDPY02). L. X. holds the Jiangsu Specially-Appointed Professorship.

## References

- 1 R. B. Song, W. Zhu, J. Fu, Y. Chen, L. Liu, J. R. Zhang, Y. Lin and J. J. Zhu, Electrode Materials Engineering in Electrocatalytic CO<sub>2</sub> Reduction: Energy Input and Conversion Efficiency, *Adv. Mater.*, 2020, **32**, 1903796.
- 2 H. Q. Liang, T. Beweries, R. Francke and M. Beller, Molecular Catalysts for the Reductive Homocoupling of CO<sub>2</sub> towards C<sub>2+</sub> Compounds, *Angew. Chem., Int. Ed.*, 2022, **61**, e202200723.

- 3 M. Lu, M. Zhang, J. Liu, Y. Chen, J. P. Liao, M. Y. Yang, Y. P. Cai, S. L. Li and Y. Q. Lan, Covalent Organic Framework Based Functional Materials: Important Catalysts for Efficient CO<sub>2</sub> Utilization, *Angew. Chem., Int. Ed.*, 2022, **61**, e202200003.
- 4 B. B. Mulik, B. D. Bankar, A. V. Munde, A. V. Biradar and B. R. Sathe, Bismuth-Oxide-Decorated Graphene Oxide Hybrids for Catalytic and Electrocatalytic Reduction of CO<sub>2</sub>, *Chem. – Eur. J.*, 2020, **26**, 8801–8809.
- 5 H. Liu, Y. Zhu, J. Ma, Z. Zhang and W. Hu, Recent Advances in Atomic-Level Engineering of Nanostructured Catalysts for Electrochemical CO<sub>2</sub> Reduction, *Adv. Funct. Mater.*, 2020, **30**, 1910534.
- 6 G. Wen, B. Ren, Y. Zheng, M. Li, C. Silva, S. Song, Z. Zhang, H. Dou, L. Zhao, D. Luo, A. Yu and Z. Chen, Engineering Electrochemical Surface for Efficient Carbon Dioxide Upgrade, *Adv. Energy Mater.*, 2021, **12**, 2103289.
- 7 Y. H. Li, P. F. Liu, C. Li and H. G. Yang, Sharp-Tipped Zinc Nanowires as an Efficient Electrocatalyst for Carbon Dioxide Reduction, *Chem. – Eur. J.*, 2018, **24**, 15486–15490.
- 8 Y. Li, N. M. Adli, W. Shan, M. Wang, M. J. Zachman, S. Hwang, H. Tabassum, S. Karakalos, Z. Feng, G. Wang, Y. C. Li and G. Wu, Atomically dispersed single Ni site catalysts for high-efficiency CO<sub>2</sub> electroreduction at industrial-level current densities, *Energy Environ. Sci.*, 2022, **15**, 2108–2119.
- 9 S. Zhen, G. Zhang, D. Cheng, H. Gao, L. Li, X. Lin, Z. Ding, Z. J. Zhao and J. Gong, Nature of the Active Sites of Copper Zinc Catalysts for Carbon Dioxide Electroreduction, *Angew. Chem., Int. Ed.*, 2022, **61**, e202201913.
- 10 K. Li, S. Zhang, X. Zhang, S. Liu, H. Jiang, T. Jiang, C. Shen, Y. Yu and W. Chen, Atomic Tuning of Single-Atom Fe-N-C Catalysts with Phosphorus for Robust Electrochemical CO<sub>2</sub> Reduction, *Nano Lett.*, 2022, **22**, 1557–1565.
- 11 J. Fu, P. Li, Y. Lin, H. Du, H. Liu, W. Zhu and H. Ren, Fight for carbon neutrality with state-of-the-art negative carbon emission technologies, *Eco-Environ. Health*, 2022, **1**, 259–279.
- 12 X. Xie, X. Zhang, M. Xie, L. Xiong, H. Sun, Y. Lu, Q. Mu, M. H. Rummeli, J. Xu, S. Li, J. Zhong, Z. Deng, B. Ma, T. Cheng, W. A. Goddard, 3rd and Y. Peng, Au-activated N motifs in non-coherent cupric porphyrin metal organic frameworks for promoting and stabilizing ethylene production, *Nat. Commun.*, 2022, **13**, 63.
- 13 Y. Wu, S. Cao, J. Hou, Z. Li, B. Zhang, P. Zhai, Y. Zhang and L. Sun, Rational Design of Nanocatalysts with Nonmetal Species Modification for Electrochemical CO<sub>2</sub> Reduction, *Adv. Energy Mater.*, 2020, **10**, 2000588.
- 14 N. Li, X. Wang, X. Lu, P. Zhang and W. J. Ong, Comprehensive Mechanism of CO<sub>2</sub> Electroreduction on Non-Noble Metal Single-Atom Catalysts of Mo<sub>2</sub>CS<sub>2</sub>-MXene, *Chem. – Eur. J.*, 2021, **27**, 17900–17909.
- 15 H. Seo, M. Rahimi and T. A. Hatton, Electrochemical Carbon Dioxide Capture and Release with a Redox-Active Amine, *J. Am. Chem. Soc.*, 2022, **144**, 2164–2170.
- 16 D. D. Zhu, J. L. Liu and S. Z. Qiao, Recent Advances in Inorganic Heterogeneous Electrocatalysts for Reduction of Carbon Dioxide, *Adv. Mater.*, 2016, **28**, 3423–3452.
- 17 J. Liu, P. Li, J. Bi, Q. Zhu and B. Han, Design and Preparation of Electrocatalysts by Electrodeposition for CO<sub>2</sub> Reduction, *Chem. – Eur. J.*, 2022, **28**, e202200242.
- 18 X. Wang, Q. Zhao, B. Yang, Z. Li, Z. Bo, K. H. Lam, N. M. Adli, L. Lei, Z. Wen, G. Wu and Y. Hou, Emerging nanostructured carbon-based non-precious metal electrocatalysts for selective electrochemical CO<sub>2</sub> reduction to CO, *J. Mater. Chem. A*, 2019, **7**, 25191–25202.
- 19 D. Gao, R. M. Arán-Ais, H. S. Jeon and B. Roldan Cuenya, Rational catalyst and electrolyte design for CO<sub>2</sub> electroreduction towards multicarbon products, *Nat. Catal.*, 2019, **2**, 198–210.
- 20 S. Liang, L. Huang, Y. Gao, Q. Wang and B. Liu, Electrochemical Reduction of CO<sub>2</sub> to CO over Transition Metal/N-Doped Carbon Catalysts: The Active Sites and Reaction Mechanism, *Adv. Sci.*, 2021, **8**, 2102886.
- 21 D. M. Koshy, S. Chen, D. U. Lee, M. B. Stevens, A. M. Abdellah, S. M. Dull, G. Chen, D. Nordlund, A. Gallo, C. Hahn, D. C. Higgins, Z. Bao and T. F. Jaramillo, Understanding the Origin of Highly Selective CO<sub>2</sub> Electroreduction to CO on Ni,N-doped Carbon Catalysts, *Angew. Chem., Int. Ed.*, 2020, **59**, 4043–4050.
- 22 Y. Yan, L. Ke, Y. Ding, Y. Zhang, K. Rui, H. Lin and J. Zhu, Recent advances in Cu-based catalysts for electroreduction of carbon dioxide, *Mater. Chem. Front.*, 2021, **5**, 2668–2683.
- 23 Y. Liu, S. Chen, X. Quan and H. Yu, Efficient Electrochemical Reduction of Carbon Dioxide to Acetate on Nitrogen-Doped Nanodiamond, *J. Am. Chem. Soc.*, 2015, **137**, 11631–11636.
- 24 J. Wu, S. Ma, J. Sun, J. I. Gold, C. Tiwary, B. Kim, L. Zhu, N. Chopra, I. N. Odeh, R. Vajtai, A. Z. Yu, R. Luo, J. Lou, G. Ding, P. J. Kenis and P. M. Ajayan, A metal-free electrocatalyst for carbon dioxide reduction to multi-carbon hydrocarbons and oxygenates, *Nat. Commun.*, 2016, **7**, 13869.
- 25 L. Zhang, Z. J. Zhao and J. Gong, Nanostructured Materials for Heterogeneous Electrocatalytic CO<sub>2</sub> Reduction and their Related Reaction Mechanisms, *Angew. Chem., Int. Ed.*, 2017, **56**, 11326–11353.
- 26 B. Zhang and J. Zhang, Rational design of Cu-based electrocatalysts for electrochemical reduction of carbon dioxide, *J. Energy Chem.*, 2017, **26**, 1050–1066.
- 27 J. Liu, Y. Cai, R. Song, S. Ding, Z. Lyu, Y. Chang, H. Tian, X. Zhang, D. Du, W. Zhu, Y. Zhou and Y. Lin, Recent progress on single-atom catalysts for CO<sub>2</sub> electroreduction, *Mater. Today*, 2021, **48**, 95–114.
- 28 Y. Cai, J. Fu, Y. Zhou, Y. Chang, Q. Min, J. Zhu, Y. Lin and W. Zhu, Insights on forming N,O-coordinated Cu single-atom catalysts for electrochemical reduction CO<sub>2</sub> to methane, *Nat. Commun.*, 2021, **12**, 586.
- 29 L. Liu, Y. Zhou, Y. Chang, J. Zhang, L. Jiang, W. Zhu and Y. Lin, Tuning Sn<sub>3</sub>O<sub>4</sub> for CO<sub>2</sub> reduction to formate with ultra-high current density, *Nano Energy*, 2020, **77**, 105296.
- 30 L. Liu, J. Fu, L. Jiang, J. Zhang, W. Zhu and Y. Lin, Highly Efficient Photoelectrochemical Reduction of CO<sub>2</sub> at Low Applied Voltage Using 3D Co-Pi/BiVO<sub>4</sub>/SnO<sub>2</sub> Nanosheet



- Array Photoanodes, *ACS Appl. Mater. Interfaces*, 2019, **11**, 26024–26031.
- 31 S. Mu, Q. Shi, C. Chen, X. Gong and H. Xue, Nanopolyaniline enables highly efficient electrocatalytic reduction of CO<sub>2</sub> to methanol in supporting electrolyte-free media and the detection of free-radical signals, *Mater. Chem. Front.*, 2023, **7**, 1385–1394.
- 32 J. Liu, J. Fu, Y. Zhou, W. Zhu, L. Jiang and Y. Lin, Controlled Synthesis of EDTA-Modified Porous Hollow Copper Microspheres for High-Efficiency Conversion of CO<sub>2</sub> to Multicarbon Products, *Nano Lett.*, 2020, **20**, 4823–4828.
- 33 Y. Guan, J. Yan, Y. Liu, F. Ning, J. Yi and J. Zhang, Zn-In-O electrocatalysts with co-existing ZnO and In<sub>2</sub>O<sub>3</sub> phases for efficient reduction of CO<sub>2</sub> to formate through sacrificial mechanism, *J. Catal.*, 2023, **424**, 211–220.
- 34 F. M. Stuardi, A. Tiozzo, L. Rotundo, J. Leclaire, R. Gobetto and C. Nervi, Efficient Electrochemical Reduction of CO<sub>2</sub> to Formate in Methanol Solutions by Mn-Functionalized Electrodes in the Presence of Amines, *Chem. – Eur. J.*, 2022, **28**, e202104377.
- 35 G. Shi, Y. Xie, L. Du, X. Fu, X. Chen, W. Xie, T. B. Lu, M. Yuan and M. Wang, Constructing Cu-C Bonds in a Graphdiyne-Regulated Cu Single-Atom Electrocatalyst for CO<sub>2</sub> Reduction to CH<sub>4</sub>, *Angew. Chem., Int. Ed.*, 2022, **61**, e202203569.
- 36 M. C. O. Monteiro, F. Dattila, B. Hagedoorn, R. García-Muelas, N. López and M. T. M. Koper, Absence of CO<sub>2</sub> electroreduction on copper, gold and silver electrodes without metal cations in solution, *Nat. Catal.*, 2021, **4**, 654–662.
- 37 B. Yang, K. Liu, H. Li, C. Liu, J. Fu, H. Li, J. E. Huang, P. Ou, T. Alkayyali, C. Cai, Y. Duan, H. Liu, P. An, N. Zhang, W. Li, X. Qiu, C. Jia, J. Hu, L. Chai, Z. Lin, Y. Gao, M. Miyauchi, E. Cortes, S. A. Maier and M. Liu, Accelerating CO<sub>2</sub> Electroreduction to Multicarbon Products *via* Synergistic Electric-Thermal Field on Copper Nanoneedles, *J. Am. Chem. Soc.*, 2022, **144**, 3039–3049.
- 38 D. Bagchi, J. Raj, A. K. Singh, A. Cherevotan, S. Roy, K. S. Manoj, C. P. Vinod and S. C. Peter, Structure-Tailored Surface Oxide on Cu-Ga Intermetallics Enhances CO<sub>2</sub> Reduction Selectivity to Methanol at Ultralow Potential, *Adv. Mater.*, 2022, **34**, e2109426.
- 39 J. Chen, T. Wang, X. Wang, B. Yang, X. Sang, S. Zheng, S. Yao, Z. Li, Q. Zhang, L. Lei, J. Xu, L. Dai and Y. Hou, Promoting Electrochemical CO<sub>2</sub> Reduction *via* Boosting Activation of Adsorbed Intermediates on Iron Single-Atom Catalyst, *Adv. Funct. Mater.*, 2022, **32**, 2110174.
- 40 L. Sun, V. Reddu, A. C. Fisher and X. Wang, Electrocatalytic reduction of carbon dioxide: opportunities with heterogeneous molecular catalysts, *Energy Environ. Sci.*, 2020, **13**, 374–403.
- 41 L. Wang, W. Chen, D. Zhang, Y. Du, R. Amal, S. Qiao, J. Wu and Z. Yin, Surface strategies for catalytic CO<sub>2</sub> reduction: from two-dimensional materials to nanoclusters to single atoms, *Chem. Soc. Rev.*, 2019, **48**, 5310–5349.
- 42 T. Ouyang, S. Huang, X. T. Wang and Z. Q. Liu, Nanostructures for Electrocatalytic CO<sub>2</sub> Reduction, *Chem. – Eur. J.*, 2020, **26**, 14024–14035.
- 43 K. Lei and B. Yu Xia, Electrocatalytic CO<sub>2</sub> Reduction: from Discrete Molecular Catalysts to Their Integrated Catalytic Materials, *Chem. – Eur. J.*, 2022, **28**, e202200141.
- 44 F. Pan and Y. Yang, Designing CO<sub>2</sub> reduction electrode materials by morphology and interface engineering, *Energy Environ. Sci.*, 2020, **13**, 2275–2309.
- 45 F. Naseem, P. Lu, J. Zeng, Z. Lu, Y. H. Ng, H. Zhao, Y. Du and Z. Yin, Solid Nanoporosity Governs Catalytic CO<sub>2</sub> and N<sub>2</sub> Reduction, *ACS Nano*, 2020, **14**, 7734–7759.
- 46 Y. J. Sa, C. W. Lee, S. Y. Lee, J. Na, U. Lee and Y. J. Hwang, Catalyst-electrolyte interface chemistry for electrochemical CO<sub>2</sub> reduction, *Chem. Soc. Rev.*, 2020, **49**, 6632–6665.
- 47 H. Li, N. Xiao, M. Hao, X. Song, Y. Wang, Y. Ji, C. Liu, C. Li, Z. Guo, F. Zhang and J. Qiu, Efficient CO<sub>2</sub> electroreduction over pyridinic-N active sites highly exposed on wrinkled porous carbon nanosheets, *Chem. Eng. J.*, 2018, **351**, 613–621.
- 48 T. Zheng, C. Liu, C. Guo, M. Zhang, X. Li, Q. Jiang, W. Xue, H. Li, A. Li, C. W. Pao, J. Xiao, C. Xia and J. Zeng, Copper-catalysed exclusive CO<sub>2</sub> to pure formic acid conversion *via* single-atom alloying, *Nat. Nanotechnol.*, 2021, **16**, 1386–1393.
- 49 X. Ma, Y. Shen, S. Yao, M. Shu, R. Si and C. An, Self-Supported Nanoporous Au<sub>3</sub> Cu Electrode with Enriched Gold on Surface for Efficient Electrochemical Reduction of CO<sub>2</sub>, *Chem. – Eur. J.*, 2020, **26**, 4143–4149.
- 50 X. Lv, L. Shang, S. Zhou, S. Li, Y. Wang, Z. Wang, T. K. Sham, C. Peng and G. Zheng, Electron-Deficient Cu Sites on Cu<sub>3</sub>Ag<sub>1</sub> Catalyst Promoting CO<sub>2</sub> Electroreduction to Alcohols, *Adv. Energy Mater.*, 2020, **10**, 2001987.
- 51 S. Tang, J. Xu, X. Liu and Y. Zhu, Ag Doped Au<sub>44</sub> Nanoclusters for Electrocatalytic Conversion of CO<sub>2</sub> to CO, *Chem. – Eur. J.*, 2022, **28**, e202201262.
- 52 X. Sun, L. Lu, Q. Zhu, C. Wu, D. Yang, C. Chen and B. Han, MoP Nanoparticles Supported on Indium-Doped Porous Carbon: Outstanding Catalysts for Highly Efficient CO<sub>2</sub> Electroreduction, *Angew. Chem., Int. Ed.*, 2018, **57**, 2427–2431.
- 53 G. G. Chang, X. C. Ma, Y. X. Zhang, L. Y. Wang, G. Tian, J. W. Liu, J. Wu, Z. Y. Hu, X. Y. Yang and B. Chen, Construction of Hierarchical Metal-Organic Frameworks by Competitive Coordination Strategy for Highly Efficient CO<sub>2</sub> Conversion, *Adv. Mater.*, 2019, **31**, 1904969.
- 54 Z. Xin, Y.-R. Wang, Y. Chen, W.-L. Li, L.-Z. Dong and Y.-Q. Lan, Metallocene implanted metalloporphyrin organic framework for highly selective CO<sub>2</sub> electroreduction, *Nano Energy*, 2020, **67**, 104233.
- 55 Z. Wang, Y. Zhou, D. Liu, R. Qi, C. Xia, M. Li, B. You and B. Y. Xia, Carbon-Confined Indium Oxides for Efficient Carbon Dioxide Reduction in a Solid-State Electrolyte Flow Cell, *Angew. Chem., Int. Ed.*, 2022, **61**, e202200552.
- 56 B. Chen, B. Li, Z. Tian, W. Liu, W. Liu, W. Sun, K. Wang, L. Chen and J. Jiang, Enhancement of Mass Transfer for Facilitating Industrial-Level CO<sub>2</sub> Electroreduction on Atomic Ni-N<sub>4</sub> Sites, *Adv. Energy Mater.*, 2021, **11**, 2102152.

- 57 X. Duan, J. Xu, Z. Wei, J. Ma, S. Guo, S. Wang, H. Liu and S. Dou, Metal-Free Carbon Materials for CO<sub>2</sub> Electrochemical Reduction, *Adv. Mater.*, 2017, **29**, 1701784.
- 58 S. Jin, Z. Hao, K. Zhang, Z. Yan and J. Chen, Advances and Challenges for the Electrochemical Reduction of CO<sub>2</sub> to CO: From Fundamentals to Industrialization, *Angew. Chem., Int. Ed.*, 2021, **60**, 20627–20648.
- 59 S. Navarro-Jaén, M. Virginie, J. Bonin, M. Robert, R. Wojcieszak and A. Y. Khodakov, Highlights and challenges in the selective reduction of carbon dioxide to methanol, *Nat. Rev. Chem.*, 2021, **5**, 564–579.
- 60 T. Wang, Q. Zhao, Y. Fu, C. Lei, B. Yang, Z. Li, L. Lei, G. Wu and Y. Hou, Carbon-Rich Nonprecious Metal Single Atom Electrocatalysts for CO<sub>2</sub> Reduction and Hydrogen Evolution, *Small Methods*, 2019, **3**, 1900210.
- 61 S. Nitopi, E. Bertheussen, S. B. Scott, X. Liu, A. K. Engstfeld, S. Horch, B. Seger, I. E. L. Stephens, K. Chan, C. Hahn, J. K. Nørskov, T. F. Jaramillo and I. Chorkendorff, Progress and Perspectives of Electrochemical CO<sub>2</sub> Reduction on Copper in Aqueous Electrolyte, *Chem. Rev.*, 2019, **119**, 7610–7672.
- 62 T. Xia, Z. Wang and F. Li, Seeing is believing: In-situ visualising dynamic evolution in CO<sub>2</sub> electrolysis, *Curr. Opin. Electrochem.*, 2022, **31**, 100846.
- 63 P. Saha, S. Amanullah and A. Dey, Selectivity in Electrochemical CO<sub>2</sub> Reduction, *Acc. Chem. Res.*, 2022, **55**, 134–144.
- 64 F. Pana and Y. Yang, Designing CO<sub>2</sub> reduction electrode materials by morphology and interface engineering, *Energy Environ. Sci.*, 2020, **13**, 2275–2309.
- 65 L. Wang, H. Peng, S. Lamaison, Z. Qi, D. M. Koshy, M. B. Stevens, D. Wakerley, J. A. Zamora Zeledón, L. A. King, L. Zhou, Y. Lai, M. Fontecave, J. Gregoire, F. Abild-Pedersen, T. F. Jaramillo and C. Hahn, Bimetallic effects on Zn-Cu electrocatalysts enhance activity and selectivity for the conversion of CO<sub>2</sub> to CO, *Chem. Catal.*, 2021, **1**, 663–680.
- 66 L. P. Chi, Z. Z. Niu, X. L. Zhang, P. P. Yang, J. Liao, F. Y. Gao, Z. Z. Wu, K. B. Tang and M. R. Gao, Stabilizing indium sulfide for CO<sub>2</sub> electroreduction to formate at high rate by zinc incorporation, *Nat. Commun.*, 2021, **12**, 5835.
- 67 L. C. Pardo Pérez, A. Arndt, S. Stojković, I. Y. Ahmet, J. T. Arens, F. Dattila, R. Wendt, A. Guilherme Buzanich, M. Radtke, V. Davies, K. Höflich, E. Köhnen, P. Tockhorn, R. Golnak, J. Xiao, G. Schuck, M. Wollgarten, N. López and M. T. Mayer, Determining Structure-Activity Relationships in Oxide Derived Cu-Sn Catalysts During CO<sub>2</sub> Electroreduction Using X-Ray Spectroscopy, *Adv. Energy Mater.*, 2021, **12**, 2103328.
- 68 H. Yang, Y. w Hu, J. j Chen, M. S. Balogun, P. p Fang, S. Zhang, J. Chen and Y. Tong, Intermediates Adsorption Engineering of CO<sub>2</sub> Electroreduction Reaction in Highly Selective Heterostructure Cu-Based Electrocatalysts for CO Production, *Adv. Energy Mater.*, 2019, **9**, 1901396.
- 69 Y. Mun, S. Lee, A. Cho, S. Kim, J. W. Han and J. Lee, Cu-Pd alloy nanoparticles as highly selective catalysts for efficient electrochemical reduction of CO<sub>2</sub> to CO, *Appl. Catal., B*, 2019, **246**, 82–88.
- 70 J. Zhang, T. Fan, P. Huang, X. Lian, Y. Guo, Z. Chen and X. Yi, Electro-Reconstruction-Induced Strain Regulation and Synergism of Ag-In-S toward Highly Efficient CO<sub>2</sub> Electrolysis to Formate, *Adv. Funct. Mater.*, 2022, **32**, 2113075.
- 71 M. Weller, T. Overton, J. Rourke and F. Armstrong, *Inorganic Chemistry*, Oxford University Press, Oxford, 7th edn, 2018.
- 72 S. Yan, C. Peng, C. Yang, Y. Chen, J. Zhang, A. Guan, X. Lv, H. Wang, Z. Wang, T. K. Sham, Q. Han and G. Zheng, Electron Localization and Lattice Strain Induced by Surface Lithium Doping Enable Ampere-Level Electrosynthesis of Formate from CO<sub>2</sub>, *Angew. Chem., Int. Ed.*, 2021, **60**, 25741–25745.
- 73 M. Xie, Y. Shen, W. Ma, D. Wei, B. Zhang, Z. Wang, Y. Wang, Q. Zhang, S. Xie, C. Wang and Y. Wang, Fast Screening for Copper-Based Bimetallic Electrocatalysts: Efficient Electrocatalytic Reduction of CO<sub>2</sub> to C<sub>2+</sub> Products on Magnesium-Modified Copper, *Angew. Chem., Int. Ed.*, 2022, **61**, e202213423, DOI: [10.1002/anie.202213423](https://doi.org/10.1002/anie.202213423).
- 74 A. Xu, S. Hung, A. Cao, Z. Wang, N. Karmodak, J. E. Huang, Y. Yan, A. S. Rasouli, A. Ozden, F. Wu, Z. Lin, H. Tsai, T. Lee, F. Li, M. Luo, Y. Wang, X. Wang, J. Abed, Z. Wang, D. Nam, Y. C. Li, A. H. Ip, D. Sinton, C. Dong and E. H. Sargent, Copper/alkaline earth metal oxide interfaces for electrochemical CO<sub>2</sub>-to-alcohol conversion by selective hydrogenation, *Nat. Catal.*, 2022, **5**, 1081–1088.
- 75 W. Dan, K. Chang, Y. Zhang, Y. Wang, Q. Liu, Z. Wang, D. Ding, Y. Cui, C. Pan, Y. Lou, Y. Zhu and Y. Zhang, Unravelling the electrocatalytic activity of bismuth nanosheets towards carbon dioxide reduction: Edge plane versus basal plane, *Appl. Catal., B*, 2021, **299**, 120693.
- 76 Q. Li, X. Rao, J. Sheng, J. Xu, J. Yi, Y. Liu and J. Zhang, Energy storage through CO<sub>2</sub> electroreduction: A brief review of advanced Sn-based electrocatalysts and electrodes, *J. CO<sub>2</sub> Util.*, 2018, **27**, 48–59.
- 77 H. Shang, T. Wang, J. Pei, Z. Jiang, D. Zhou, Y. Wang, H. Li, J. Dong, Z. Zhuang, W. Chen, D. Wang, J. Zhang and Y. Li, Design of a Single-Atom Indium<sup>δ+</sup>-N<sub>4</sub> Interface for Efficient Electroreduction of CO<sub>2</sub> to Formate, *Angew. Chem., Int. Ed.*, 2020, **59**, 22465–22469.
- 78 Y. Shi, Y. Ji, J. Long, Y. Liang, Y. Liu, Y. Yu, J. Xiao and B. Zhang, Unveiling hydrocerussite as an electrochemically stable active phase for efficient carbon dioxide electroreduction to formate, *Nat. Commun.*, 2020, **11**, 3415.
- 79 F. Yang, X. Ma, W. B. Cai, P. Song and W. Xu, Nature of Oxygen-Containing Groups on Carbon for High-Efficiency Electrocatalytic CO<sub>2</sub> Reduction Reaction, *J. Am. Chem. Soc.*, 2019, **141**, 20451–20459.
- 80 X. An, S. Li, A. Yoshida, T. Yu, Z. Wang, X. Hao, A. Abudula and G. Guan, Bi-Doped SnO Nanosheets Supported on Cu Foam for Electrochemical Reduction of CO<sub>2</sub> to HCOOH, *ACS Appl. Mater. Interfaces*, 2019, **11**, 42114–42122.
- 81 X. Li, X. Wu, J. Li, J. Huang, L. Ji, Z. Leng, N. Qian, D. Yang and H. Zhang, Sn-Doped Bi<sub>2</sub>O<sub>3</sub> nanosheets for highly

- efficient electrochemical CO<sub>2</sub> reduction toward formate production, *Nanoscale*, 2021, **13**, 19610–19616.
- 82 M. Wu, Y. Xiong, B. Hu, Z. Zhang, B. Wei, L. Li, J. Hao and W. Shi, Indium doped bismuth subcarbonate nanosheets for efficient electrochemical reduction of carbon dioxide to formate in a wide potential window, *J. Colloid Interface Sci.*, 2022, **624**, 261–269.
- 83 G. Wen, D. U. Lee, B. Ren, F. M. Hassan, G. Jiang, Z. P. Cano, J. Gostick, E. Croiset, Z. Bai, L. Yang and Z. Chen, Orbital Interactions in Bi-Sn Bimetallic Electrocatalysts for Highly Selective Electrochemical CO<sub>2</sub> Reduction toward Formate Production, *Adv. Energy Mater.*, 2018, **8**, 1802427.
- 84 B. Ren, G. Wen, R. Gao, D. Luo, Z. Zhang, W. Qiu, Q. Ma, X. Wang, Y. Cui, L. Ricardez-Sandoval, A. Yu and Z. Chen, Nano-crumpled induced Sn-Bi bimetallic interface pattern with moderate electron bank for highly efficient CO<sub>2</sub> electroreduction, *Nat. Commun.*, 2022, **13**, 2486.
- 85 J. Tang, R. Daiyan, M. B. Ghasemian, S. A. Idrus-Saidi, A. Zavabeti, T. Daeneke, J. Yang, P. Koshy, S. Cheong, R. D. Tilley, R. B. Kaner, R. Amal and K. Kalantar-Zadeh, Advantages of eutectic alloys for creating catalysts in the realm of nanotechnology-enabled metallurgy, *Nat. Commun.*, 2019, **10**, 4645.
- 86 Z. Wu, H. Wu, W. Cai, Z. Wen, B. Jia, L. Wang, W. Jin and T. Ma, Engineering Bismuth-Tin Interface in Bimetallic Aerogel with a 3D Porous Structure for Highly Selective Electrocatalytic CO<sub>2</sub> Reduction to HCOOH, *Angew. Chem., Int. Ed.*, 2021, **60**, 12554–12559.
- 87 Z. Wu, H. Wu, W. Cai, Z. Wen, B. Jia, L. Wang, W. Jin and T. Ma, Engineering Bismuth-Tin Interface in Bimetallic Aerogel with a 3D Porous Structure for Highly Selective Electrocatalytic CO<sub>2</sub> Reduction to HCOOH, *Angew. Chem., Int. Ed.*, 2021, **60**, 12554–12559.
- 88 J. Wang, S. Ning, M. Luo, D. Xiang, W. Chen, X. Kang, Z. Jiang and S. Chen, In-Sn alloy core-shell nanoparticles: In-doped SnOx shell enables high stability and activity towards selective formate production from electrochemical reduction of CO<sub>2</sub>, *Appl. Catal., B*, 2021, **288**, 119979.
- 89 Y. Guan, X. Zhang, Y. Zhang, T. N. V. Karsili, M. Fan, Y. Liu, B. Marchetti and X. D. Zhou, Achieving high selectivity towards electro-conversion of CO<sub>2</sub> using In-doped Bi derived from metal-organic frameworks, *J. Colloid Interface Sci.*, 2022, **612**, 235–245.
- 90 L. Liu, X. Li, Y. Cai, H. Du, F. Liu, J. Zhang, J. Fu and W. Zhu, Hierarchical S-modified Cu porous nanoflakes for efficient CO<sub>2</sub> electroreduction to formate, *Nanoscale*, 2022, **14**, 13679–13688.
- 91 G. A. Lawrance, *Introduction to Coordination Chemistry*, Wiley, Chichester, 2010.
- 92 H. B. Yang, S.-F. Hung, S. Liu, K. Yuan, S. Miao, L. Zhang, X. Huang, H.-Y. Wang, W. Cai, R. Chen, J. Gao, X. Yang, W. Chen, Y. Huang, H. M. Chen, C. M. Li, T. Zhang and B. Liu, Atomically dispersed Ni(i) as the active site for electrochemical CO<sub>2</sub> reduction, *Nat. Energy*, 2018, **3**, 140–147.
- 93 Y. Wu, C. Chen, X. Yan, X. Sun, Q. Zhu, P. Li, Y. Li, S. Liu, J. Ma, Y. Huang and B. Han, Boosting CO<sub>2</sub> Electroreduction over a Cadmium Single-Atom Catalyst by Tuning of the Axial Coordination Structure, *Angew. Chem., Int. Ed.*, 2021, **60**, 20803–20810.
- 94 Y. Cheng, S. Zhao, H. Li, S. He, J.-P. Veder, B. Johannessen, J. Xiao, S. Lu, J. Pan, M. F. Chisholm, S.-Z. Yang, C. Liu, J. G. Chen and S. P. Jiang, Unsaturated edge-anchored Ni single atoms on porous microwave exfoliated graphene oxide for electrochemical CO<sub>2</sub>, *Appl. Catal., B*, 2019, **243**, 294–303.
- 95 S. Dieckhofer, D. Ohl, J. R. C. Junqueira, T. Quast, T. Turek and W. Schuhmann, Probing the Local Reaction Environment During High Turnover Carbon Dioxide Reduction with Ag-Based Gas Diffusion Electrodes, *Chem. – Eur. J.*, 2021, **27**, 5906–5912.
- 96 J. Gu, C. S. Hsu, L. Bai, H. M. Chen and X. Hu, Atomically dispersed Fe<sup>3+</sup> sites catalyze efficient CO<sub>2</sub> electroreduction to CO, *Science*, 2019, **364**, 1091–1094.
- 97 L. Lin, H. Li, Y. Wang, H. Li, P. Wei, B. Nan, R. Si, G. Wang and X. Bao, Temperature-Dependent CO<sub>2</sub> Electroreduction over Fe-N-C and Ni-N-C Single-Atom Catalysts, *Angew. Chem., Int. Ed.*, 2021, **60**, 26582–26586.
- 98 J. D. Yi, R. Xie, Z. L. Xie, G. L. Chai, T. F. Liu, R. P. Chen, Y. B. Huang and R. Cao, Highly Selective CO<sub>2</sub> Electroreduction to CH<sub>4</sub> by In Situ Generated Cu<sub>2</sub>O Single-Type Sites on a Conductive MOF: Stabilizing Key Intermediates with Hydrogen Bonding, *Angew. Chem., Int. Ed.*, 2020, **59**, 23641–23648.
- 99 H. Sun, L. Chen, L. Xiong, K. Feng, Y. Chen, X. Zhang, X. Yuan, B. Yang, Z. Deng, Y. Liu, M. H. Rummeli, J. Zhong, Y. Jiao and Y. Peng, Promoting ethylene production over a wide potential window on Cu crystallites induced and stabilized *via* current shock and charge delocalization, *Nat. Commun.*, 2021, **12**, 6823.
- 100 J. Y. Kim, G. Kim, H. Won, I. Gereige, W. B. Jung and H. T. Jung, Synergistic Effect of Cu<sub>2</sub>O Mesh Pattern on High-Facet Cu Surface for Selective CO<sub>2</sub> Electroreduction to Ethanol, *Adv. Mater.*, 2022, **34**, 2106028.
- 101 Z. Li, D. He, X. Yan, S. Dai, S. Younan, Z. Ke, X. Pan, X. Xiao, H. Wu and J. Gu, Size-Dependent Nickel-Based Electrocatalysts for Selective CO<sub>2</sub> Reduction, *Angew. Chem., Int. Ed.*, 2020, **59**, 18572–18577.
- 102 W. Liu, Z. Miao, Z. Li, X. Wu, P. Zhou, J. Zhao, H. Zhao, W. Si, J. Zhou and S. Zhuo, Electroreduction of CO<sub>2</sub> catalyzed by Co@N-C materials, *J. CO<sub>2</sub> Util.*, 2019, **32**, 241–250.
- 103 S. Li, S. Zhao, X. Lu, M. Ceccato, X. M. Hu, A. Roldan, J. Catalano, M. Liu, T. Skrydstrup and K. Daasbjerg, Low-Valence Zn<sup>δ+</sup> (0 < δ < 2) Single-Atom Material as Highly Efficient Electrocatalyst for CO<sub>2</sub> Reduction, *Angew. Chem., Int. Ed.*, 2021, **60**, 22826–22832.
- 104 G. Hyun, J. T. Song, C. Ahn, Y. Ham, D. Cho, J. Oh and S. Jeon, Hierarchically porous Au nanostructures with interconnected channels for efficient mass transport in electrocatalytic CO<sub>2</sub> reduction, *Proc. Natl. Acad. Sci. U. S. A.*, 2020, **117**, 5680–5685.

- 105 C. Kim, H. S. Jeon, T. Eom, M. S. Jee, H. Kim, C. M. Friend, B. K. Min and Y. J. Hwang, Achieving Selective and Efficient Electrocatalytic Activity for CO<sub>2</sub> Reduction Using Immobilized Silver Nanoparticles, *J. Am. Chem. Soc.*, 2015, **137**, 13844–13850.
- 106 S. Zhu, Q. Wang, X. Qin, M. Gu, R. Tao, B. P. Lee, L. Zhang, Y. Yao, T. Li and M. Shao, Tuning Structural and Compositional Effects in Pd-Au Nanowires for Highly Selective and Active CO<sub>2</sub> Electrochemical Reduction Reaction, *Adv. Energy Mater.*, 2018, **8**, 1802238.
- 107 A. Ozden, Y. Liu, C.-T. Dinh, J. Li, P. Ou, F. P. Garcia de Arquer, E. H. Sargent and D. Sinton, Gold Adparticles on Silver Combine Low Overpotential and High Selectivity in Electrochemical CO<sub>2</sub> Conversion, *ACS Appl. Energy Mater.*, 2021, **4**, 7504–7512.
- 108 N. Sikdar, J. R. C. Junqueira, D. Ohl, S. Dieckhofer, T. Quast, M. Braun, H. B. Aiyappa, S. Seisel, C. Andronesco and W. Schuhmann, Redox Replacement of Silver on MOF-Derived Cu/C Nanoparticles on Gas Diffusion Electrodes for Electrocatalytic CO<sub>2</sub> Reduction, *Chem. – Eur. J.*, 2022, **28**, e202104249.
- 109 Y. Hori, K. Kikuchi and S. Suzuki, Production of CO and CH<sub>4</sub> in Electrochemical Reduction of CO<sub>2</sub> at Metal Electrodes in Aqueous Hydrogencarbonate Solution, *Chem. Lett.*, 1985, 1695–1698.
- 110 B. Deng, M. Huang, K. Li, X. Zhao, Q. Geng, S. Chen, H. Xie, X. Dong, H. Wang and F. Dong, The Crystal Plane is not the Key Factor for CO<sub>2</sub>-to-Methane Electrosynthesis on Reconstructed Cu<sub>2</sub>O Microparticles, *Angew. Chem., Int. Ed.*, 2022, **61**, e202114080.
- 111 D. H. Nam, O. S. Bushuyev, J. Li, P. De Luna, A. Seifitokaldani, C. T. Dinh, F. P. Garcia de Arquer, Y. Wang, Z. Liang, A. H. Proppe, C. S. Tan, P. Todorovic, O. Shekhah, C. M. Gabardo, J. W. Jo, J. Choi, M. J. Choi, S. W. Baek, J. Kim, D. Sinton, S. O. Kelley, M. Eddaoudi and E. H. Sargent, Metal-Organic Frameworks Mediate Cu Coordination for Selective CO<sub>2</sub> Electroreduction, *J. Am. Chem. Soc.*, 2018, **140**, 11378–11386.
- 112 Y. Ma, J. Yu, M. Sun, B. Chen, X. Zhou, C. Ye, Z. Guan, W. Guo, G. Wang, S. Lu, D. Xia, Y. Wang, Z. He, L. Zheng, Q. Yun, L. Wang, J. Zhou, P. Lu, J. Yin, Y. Zhao, Z. Luo, L. Zhai, L. Liao, Z. Zhu, R. Ye, Y. Chen, Y. Lu, S. Xi, B. Huang, C. S. Lee and Z. Fan, Confined Growth of Silver-Copper Janus Nanostructures with 100 Facets for Highly Selective Tandem Electrocatalytic Carbon Dioxide Reduction, *Adv. Mater.*, 2022, **34**, 2110607.
- 113 X. Zhang, C. Liu, Y. Zhao, L. Li, Y. Chen, F. Raziq, L. Qiao, S.-X. Guo, C. Wang, G. G. Wallace, A. M. Bond and J. Zhang, Atomic nickel cluster decorated defect-rich copper for enhanced C<sub>2</sub> product selectivity in electrocatalytic CO<sub>2</sub> reduction, *Appl. Catal., B*, 2021, **291**, 120030.
- 114 F. Hu, L. Yang, Y. Jiang, C. Duan, X. Wang, L. Zeng, X. Lv, D. Duan, Q. Liu, T. Kong, J. Jiang, R. Long and Y. Xiong, Ultrastable Cu Catalyst for CO<sub>2</sub> Electroreduction to Multi-carbon Liquid Fuels by Tuning C-C Coupling with CuTi Subsurface, *Angew. Chem., Int. Ed.*, 2021, **60**, 26122–26127.
- 115 A. Rollat, J. Lucas, P. Lucas, T. L. Mercier and W. Davenport, *Rare earths: Science, Technology, Production and use*, Elsevier, Amsterdam, 2015.
- 116 W. Liu, P. Bai, S. Wei, C. Yang and L. Xu, Gadolinium Changes the Local Electron Densities of Nickel 3d Orbitals for Efficient Electrocatalytic CO<sub>2</sub> Reduction, *Angew. Chem., Int. Ed.*, 2022, **61**, e202201166.
- 117 J. Feng, L. Wu, S. Liu, L. Xu, X. Song, L. Zhang, Q. Zhu, X. Kang, X. Sun and B. Han, Improving CO<sub>2</sub>-to-C<sub>2+</sub> Product Electroreduction Efficiency via Atomic Lanthanide Dopant-Induced Tensile-Strained CuOx Catalysts, *J. Am. Chem. Soc.*, 2023, **145**, 9857–9866.
- 118 J. Zhao, P. Zhang, T. Yuan, D. Cheng, S. Zhen, H. Gao, T. Wang, Z. Zhao and J. Gong, Modulation of \*CH<sub>x</sub>O Adsorption to Facilitate Electrocatalytic Reduction of CO<sub>2</sub> to CH<sub>4</sub> over Cu-Based Catalysts, *J. Am. Chem. Soc.*, 2023, **145**, 6622–6627.
- 119 L. Liu, Y. Cai, H. Du, X. Lu, X. Li, F. Liu, J. Fu and J. Zhu, Enriching the Local Concentration of CO Intermediates on Cu Cavities for the Electrocatalytic Reduction of CO<sub>2</sub> to C<sub>2+</sub> Products, *ACS Appl. Mater. Interfaces*, 2023, **15**, 16673–16679.
- 120 W. Zhu, Y. J. Zhang, H. Zhang, H. Lv, Q. Li, R. Michalsky, A. A. Peterson and S. Sun, Active and selective conversion of CO<sub>2</sub> to CO on ultrathin Au nanowires, *J. Am. Chem. Soc.*, 2014, **136**, 16132–16135.
- 121 F. Pan, B. Li, E. Sarnello, Y. Fei, Y. Gang, X. Xiang, Z. Du, P. Zhang, G. Wang, H. T. Nguyen, T. Li, Y. H. Hu, H. C. Zhou and Y. Li, Atomically Dispersed Iron-Nitrogen Sites on Hierarchically Mesoporous Carbon Nanotube and Graphene Nanoribbon Networks for CO<sub>2</sub> Reduction, *ACS Nano*, 2020, **14**, 5506–5516.
- 122 Z. Ma, C. Tsounis, P. V. Kumar, Z. Han, R. J. Wong, C. Y. Toe, S. Zhou, N. M. Bedford, L. Thomsen, Y. H. Ng and R. Amal, Enhanced Electrochemical CO<sub>2</sub> Reduction of Cu@Cu<sub>x</sub>O Nanoparticles Decorated on 3D Vertical Graphene with Intrinsic sp<sup>3</sup>-type Defect, *Adv. Funct. Mater.*, 2020, **30**, 1910118.
- 123 W. Bi, X. Li, R. You, M. Chen, R. Yuan, W. Huang, X. Wu, W. Chu, C. Wu and Y. Xie, Surface Immobilization of Transition Metal Ions on Nitrogen-Doped Graphene Realizing High-Efficient and Selective CO<sub>2</sub> Reduction, *Adv. Mater.*, 2018, **30**, 1706617.
- 124 Y. Li, X. F. Lu, S. Xi, D. Luan, X. Wang and X. W. D. Lou, Synthesis of N-Doped Highly Graphitic Carbon Urchin-Like Hollow Structures Loaded with Single-Ni Atoms towards Efficient CO<sub>2</sub> Electroreduction, *Angew. Chem., Int. Ed.*, 2022, **61**, e202201491.
- 125 Y. Song, W. Chen, C. Zhao, S. Li, W. Wei and Y. Sun, Metal-Free Nitrogen-Doped Mesoporous Carbon for Electroreduction of CO<sub>2</sub> to Ethanol, *Angew. Chem., Int. Ed.*, 2017, **56**, 10840–10844.
- 126 W. Zhang, C. Yang, W. Liu, H. Wang, S. Wei, J. Qi, P. Bai, B. Jin and L. Xu, Long-range order, short-range disorder: Engineering one-dimensional flow channel arrays with hierarchically porous reaction interfaces for electrocatalytic reduction of oxygen, *Appl. Catal., B*, 2021, **293**, 120199.

- 127 C. Yang, P. Bai, W. Liu, S. Wei, W. Zhang and L. Xu, Optimization of pH-universal O<sub>2</sub> reduction electrocatalysis by precise control over structural variables *via* basic bathing, *Appl. Catal., B*, 2022, **303**, 120912.
- 128 W. Ni, Y. Xue, X. Zang, C. Li, H. Wang, Z. Yang and Y.-M. Yan, Fluorine Doped Cage-like Carbon Electrocatalyst: An Insight into the Structure-Enhanced CO Selectivity for CO<sub>2</sub> Reduction at High Overpotential, *ACS Nano*, 2020, **14**, 2014–2023.
- 129 J. Xie, X. Zhao, M. Wu, Q. Li, Y. Wang and J. Yao, Metal-Free Fluorine-Doped Carbon Electrocatalyst for CO<sub>2</sub> Reduction Outcompeting Hydrogen Evolution, *Angew. Chem., Int. Ed.*, 2018, **57**, 9640–9644.
- 130 F. Li, M. Xue, G. P. Knowles, L. Chen, D. R. MacFarlane and J. Zhang, Porous nitrogen-doped carbon derived from biomass for electrocatalytic reduction of CO<sub>2</sub> to CO, *Electrochim. Acta*, 2017, **245**, 561–568.
- 131 P. Yao, Y. Qiu, T. Zhang, P. Su, X. Li and H. Zhang, N-Doped Nanoporous Carbon from Biomass as a Highly Efficient Electrocatalyst for the CO<sub>2</sub> Reduction Reaction, *ACS Sustainable Chem. Eng.*, 2019, **7**, 5249–5255.
- 132 X. Hao, X. An, A. M. Patil, P. Wang, X. Ma, X. Du, X. Hao, A. Abudula and G. Guan, Biomass-Derived N-Doped Carbon for Efficient Electrocatalytic CO<sub>2</sub> Reduction to CO and Zn-CO<sub>2</sub> Batteries, *ACS Appl. Mater. Interfaces*, 2021, **13**, 3738–3747.
- 133 S. Zhang, X. Zhang, J. Zhang, H. Zheng, G. Li, K. Zeng, J. Shao, H. Yang, S. Zhang and H. Chen, Three-dimension in-situ nitrogen doping porous cellulosic biomass-based carbon aerogel for electrocatalytic CO<sub>2</sub> reduction, *Fuel Process. Technol.*, 2023, **242**, 107612.
- 134 M. Chen, S. Wang, H. Zhang, P. Zhang, Z. Tian, M. Lu, X. Xie, L. Huang and W. Huang, Intrinsic defects in biomass-derived carbons facilitate electroreduction of CO<sub>2</sub>, *Nano Res.*, 2020, **13**, 729–735.
- 135 G. Qi, Q. Zhao, Q. Liu, D. Fang and X. Liu, Biomass-derived carbon frameworks for oxygen and carbon dioxide electrochemical reduction, *Ionics*, 2021, **27**, 3579–3586.
- 136 W. Liu, J. Qi, P. Bai, W. Zhang and L. Xu, Utilizing spatial confinement effect of N atoms in micropores of coal-based metal-free material for efficiently electrochemical reduction of carbon dioxide, *Appl. Catal., B*, 2020, **272**, 118974.
- 137 W. Liu, S. Wei, P. Bai, C. Yang and L. Xu, Robust coal matrix intensifies electron/substrate interaction of nickel-nitrogen (Ni-N) active sites for efficient CO<sub>2</sub> electroreduction at industrial current density, *Appl. Catal., B*, 2021, **299**, 120661.
- 138 J. Qi, B. Jin, W. Liu, W. Zhang and L. Xu, Converting coals into carbon-based pH-universal oxygen reduction catalysts for fuel cells, *Fuel*, 2021, **285**, 119163.
- 139 J. Qi, B. Jin, P. Bai, W. Zhang and L. Xu, Template-free preparation of anthracite-based nitrogen-doped porous carbons for high-performance supercapacitors and efficient electrocatalysts for the oxygen reduction reaction, *RSC Adv.*, 2019, **9**, 24344–24356.
- 140 H. Yang, Y. Wu, Q. Lin, L. Fan, X. Chai, Q. Zhang, J. Liu, C. He and Z. Lin, Composition Tailoring *via* N and S Co-doping and Structure Tuning by Constructing Hierarchical Pores: Metal-Free Catalysts for High-Performance Electrochemical Reduction of CO<sub>2</sub>, *Angew. Chem., Int. Ed.*, 2018, **57**, 15476–15480.
- 141 X. Hao, X. An, A. M. Patil, P. Wang, X. Ma, X. Du, X. Hao, A. Abudula and G. Guan, Biomass-Derived N-Doped Carbon for Efficient Electrocatalytic CO<sub>2</sub> Reduction to CO and Zn-CO<sub>2</sub> Batteries, *ACS Appl. Mater. Interfaces*, 2021, **13**, 3738–3747.
- 142 M. Liu, S. Liu, Q. Xu, Q. Miao, S. Yang, S. Hanson, G. Z. Chen, J. He, Z. Jiang and G. Zeng, Dual atomic catalysts from COF-derived carbon for CO<sub>2</sub>RR by suppressing HER through synergistic effects., *Carbon Energy*, 2023, 1–12, DOI: [10.1002/cey2.300](https://doi.org/10.1002/cey2.300).
- 143 S. Li, Y. Kang, C. Mo, Y. Peng, H. Ma and J. Peng, Nitrogen-Doped Bismuth Nanosheet as an Efficient Electrocatalyst to CO<sub>2</sub> Reduction for Production of Formate, *Int. J. Mol. Sci.*, 2022, **23**, 14485.
- 144 Z. Xin, J. Liu, X. Wang, K. Shen, Z. Yuan, Y. Chen and Y. Q. Lan, Implanting Polypyrrole in Metal-Porphyrin MOFs: Enhanced Electrocatalytic Performance for CO<sub>2</sub>RR, *ACS Appl. Mater. Interfaces*, 2021, **13**, 54959–54966.
- 145 Y. Zhou, G. Ni, K. Wu, Q. Chen, X. Wang, W. Zhu, Z. He, H. Li, J. Fu and M. Liu, Porous Zn Conformal Coating on Dendritic-Like Ag with Enhanced Selectivity and Stability for CO<sub>2</sub> Electroreduction to CO, *Adv. Sustainable Syst.*, 2023, **7**, 2200374.
- 146 Y. Chen, L. Zou, H. Liu, C. Chen, Q. Wang, M. Gu, B. Yang, Z. Zou, J. Fang and H. Yang, Fe and N Co-Doped Porous Carbon Nanospheres with High Density of Active Sites for Efficient CO<sub>2</sub> Electroreduction, *J. Phys. Chem. C*, 2019, **123**, 16651–16659.
- 147 Y. Chen, L. Ma, C. Chen, W. Hu, L. Zou, Z. Zou and H. Yang, Fe and N co-doped carbon with High doping content of sulfur and nitrogen for efficient CO<sub>2</sub> electroreduction, *J. CO<sub>2</sub> Util.*, 2020, **42**, 101316.